iScience

CellPress
OPEN ACCESS

Article

The fission yeast FLCN/FNIP complex augments TORC1 repression or activation in response to amino acid (AA) availability

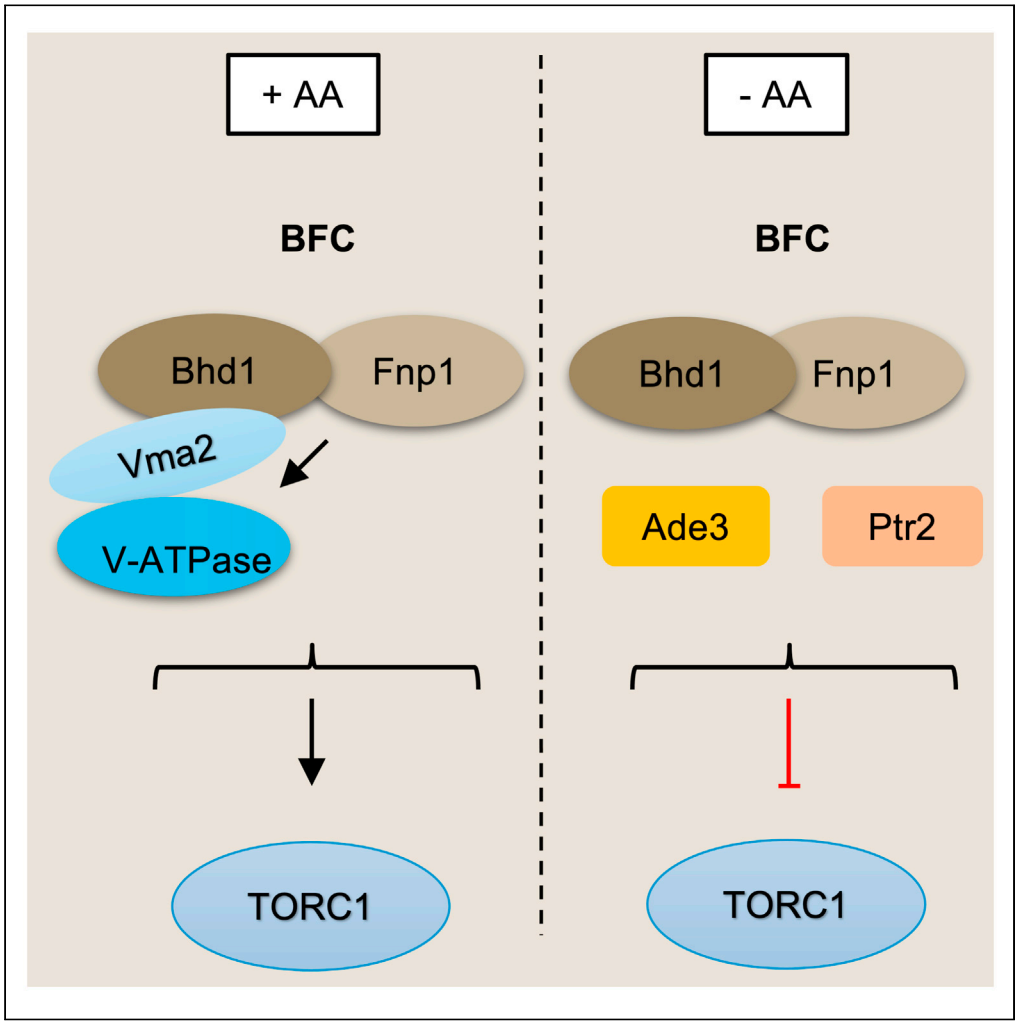

Isabel A. Calvo, Shalini Sharma, Joao A. Paulo, ..., Othon Iliopoulos, Steven P. Gygi, Mo Motamedi

mmotamedi@hms.harvard.edu

Highlights

The *S.pombe* Folliculin complex, Bhd1-Fnp1 Complex (BFC) augments repression or activation of TORC1 in response to amino acid levels, similar to a rheostat

BFC interacts and regulates V-ATPase activity in response to amino acid levels

Proteomic data reveal Ptr2 and Ade3 as novel amino acid-dependent regulators of TORC1

S. pombe is an excellent model for studying the tumor suppressor function of BFC and related proteins

Calvo et al., iScience 24, 103338
November 19, 2021
https://doi.org/10.1016/j.isci.2021.103338

iScience

CellPress
OPEN ACCESS

Article

The fission yeast FLCN/FNIP complex augments TORC1 repression or activation in response to amino acid (AA) availability

Isabel A. Calvo,[1,6,9] Shalini Sharma,[1,9] Joao A. Paulo,[2] Alexander O.D. Gulka,[1] Andras Boeszoermenyi,[3,4] Jingyu Zhang,[1] Jose M. Lombana,[1] Christina M. Palmieri,[1,7] Laura A. Laviolette,[1,8] Haribabu Arthanari,[3,4] Othon Iliopoulos,[1,5] Steven P. Gygi,[2] and Mo Motamedi[1,10,*]

SUMMARY

The target of Rapamycin complex1 (TORC1) senses and integrates several environmental signals, including amino acid (AA) availability, to regulate cell growth. Folliculin (FLCN) is a tumor suppressor (TS) protein in renal cell carcinoma, which paradoxically activates TORC1 in response to AA supplementation. Few tractable systems for modeling FLCN as a TS are available. Here, we characterize the FLCN-containing complex in *Schizosaccharomyces pombe* (called BFC) and show that BFC augments TORC1 repression and activation in response to AA starvation and supplementation, respectively. BFC co-immunoprecipitates V-ATPase, a TORC1 modulator, and regulates its activity in an AA-dependent manner. BFC genetic and proteomic networks identify the conserved peptide transmembrane transporter Ptr2 and the phosphoribosylformylglycinamidine synthase Ade3 as new AA-dependent regulators of TORC1. Overall, these data ascribe an additional repressive function to Folliculin in TORC1 regulation and reveal *S. pombe* as an excellent system for modeling the AA-dependent, FLCN-mediated repression of TORC1 in eukaryotes.

INTRODUCTION

Cellular survival requires the continuous and accurate sensing of the environment by signaling networks through which cells adjust their physiological state based on their environmental and nutritional conditions. In eukaryotes, at the center of one such signaling pathway lies the highly conserved tripartite target of rapamycin complex 1 (TORC1), whose catalytic core, TOR, is a Ser/Thr protein kinase capable of phosphorylating multiple substrates (Liu and Sabatini, 2020). TORC1 integrates a broad set of environmental signals, including the availability of amino acids, oxygen, energy, growth factors and carbon, nitrogen, and phosphate sources to regulate cellular or organismal growth (Gonzalez et al., 2020). Upon receiving growth-promoting inputs, TORC1 antagonistically promotes anabolic processes, such as protein, lipid, and nucleotide synthesis, while simultaneously repressing catabolic ones, such as autophagy. These are achieved by TOR-mediated phosphorylation and regulation of several critical downstream targets involved in multiple biological processes (Liu and Sabatini, 2020; Valvezan and Manning, 2019). Dysregulation of TORC1 signaling has been linked to several human pathologies including cancers, age-related diseases, and developmental conditions (Hua et al., 2019; Saxton and Sabatini, 2017), thus presenting an attractive target for drug development. Consistent with its importance in normal physiology, drugs targeting TOR kinase or other components of the TORC1 signaling networks have emerged as promising treatment strategies for an increasing number of medical conditions (Kato et al., 2019; Saxton and Sabatini, 2017; Sengupta et al., 2019).

Amino acid-dependent regulation of TORC1 (Hara et al., 1998; Wang et al., 1998) is an ancient growth regulatory signal that ensures the upregulation of protein synthesis is coupled with the availability of amino acids. Early studies on how amino acids regulate TORC1 activity have revealed that in response to amino acid stimulation, a complex composed of four Rag family small guanosine triphosphatases (GTPases) binds and recruits TORC1 to lysosomal surfaces (Kim et al., 2008; Rogala et al., 2019; Sancak et al., 2008), where its kinase activator, the GTP bound lysosomal Rheb, drives its activation. The Rag GTPase complex is

[1]Massachusetts General Hospital Center for Cancer Research and Department of Medicine Harvard Medical School, Charlestown, MA 02129, USA

[2]Department of Cell Biology, Harvard Medical School, Boston, MA 02115, USA

[3]Department of Biochemistry and Molecular Pharmacology, Harvard Medical School, Boston, MA 02115, USA

[4]Dana-Farber Cancer Institute, Boston, MA 02215, USA

[5]Division of Hematology-Oncology, Department of Medicine, Massachusetts General Hospital, Boston, MA 02114, USA

[6]Present address: Hematology-Oncology Program, Center for Applied Medical Research (CIMA), University of Navarra. IdiSNA and CIBERONC, Navarra, Spain

[7]Presentaddress: Spaulding Hospital for Continuing Medical Care, Cambridge, MA 02138, USA

[8]Presentaddress: Bluebird Bio, Oncology Research, Cambridge, MA, USA

[9]These authors contributed equally

[10]Lead contact

*Correspondence: mmotamedi@hms.harvard.edu

https://doi.org/10.1016/j.isci.2021.103338

composed of heterodimers of highly similar RagA or RagB bound to highly similar RagC or RagD (Hirose et al., 1998; Schurmann et al., 1995; Sekiguchi et al., 2001), which are anchored to lysosomal surfaces by the pentameric Ragulator complex (Bar-Peled et al., 2012; Nada et al., 2009; Sancak et al., 2010; Wunderlich et al., 2001). Under amino acid replete conditions, the Rag complex is converted into its active form where RagA/B is loaded with GTP and RagC/D is loaded with GDP (RagA/B·GTP-RagC/D·GDP). This is regulated by distinct guanine nucleotide exchange factors (GEFs) and GTPase activating proteins (GAPs), including the Ragulator complex, which in addition to anchoring the Rag complex, functions as a GEF on the RagA/B subunit (Bar-Peled et al., 2012). Also, the tumor suppressor FLCN-FNIP complex activates RagC/D through its GAP activity (Petit et al., 2013; Tsun et al., 2013). Together the Ragulator and FLCN/FNIP activities convert the Rag complex into its active form, which is recognized by the raptor subunit of mammalian TORC1 (mTORC1) (Rogala et al., 2019), triggering its translocation to the lysosomal surfaces (Jewell et al., 2013; Sancak et al., 2008).

In addition to these, the vacuolar-type H^+ATPase (V-ATPase) complex also plays an important role in amino acid-dependent activation of mTORC1. This complex, consisting of membrane-embedded Vo and peripheral cytosolic V1 multi-subunit domains, functions downstream of amino acid stimulation and, in addition to establishing the pH of the lysosome, transmits the amino acid signal from lysosomal lumen to mTORC1 through the Ragulator-Rag GTPase complex (Bar-Peled et al., 2012; Jewell et al., 2013; Zoncu et al., 2011). Moreover, recent studies have revealed that three putative amino acid sensors, which operate upstream of mTORC1, convey the intracellular cytosolic and lysosomal amino acid levels to mTORC1: SLC38A9, sequestrin1/2 and CASTOR1 (Liu and Sabatini, 2020). From among these, SLC38A9, a potential arginine sensor and a positive regulator of mTORC1, has homology to amino acid transporters and has been identified as a lysosomal transmembrane amino acid sensor which interacts with the Rag GTPases and the Ragulator complexes and is required for the amino acid-dependent regulation of TORC1 (Jung et al., 2015; Rebsamen et al., 2015; Wang et al., 2015; Wolfson and Sabatini, 2017).

In humans, germline mutations in *FLCN* are responsible for causing Birt-Hogg-Dubé syndrome (BHD) (Khoo et al., 2001; Nickerson et al., 2002; Schmidt et al., 2001), an autosomal dominant hereditary disorder in which patients develop several types of benign neoplasms, such as fibrofolliculomas and pulmonary cysts, and are at an increased risk of developing renal cell carcinoma (RCC) (Birt et al., 1977; Toro et al., 1999; Zbar et al., 2002). Loss-of-function mutations occurring on both *FLCN* alleles increase RCC risk, implying a tumor suppressor role for *FLCN* (Khoo et al., 2003; Vocke et al., 2005; Warren et al., 2004). FLCN is highly conserved across eukaryotes, possessing an N-terminal Longin and a C-terminal differentially expressed in normal cells and neoplasia (DENN) domain (Nookala et al., 2012). FLCN physically interacts with two highly similar proteins, FNIP1 and FNIP2 which bind to its C-terminus (Baba et al., 2006; Hasumi et al., 2008). Several studies indicated that tumors from both BHD patients and *FLCN*-null mouse models exhibit activated TORC1 signaling, consistent with a tumor suppressor role for FLCN (Baba et al., 2008; Chen et al., 2008; Hasumi et al., 2009; Wu et al., 2015). However, FLCN has been shown to activate TORC1 (Bar-Peled and Sabatini, 2014; van Slegtenhorst et al., 2007) biochemically through its GAP activity on RagC GTPase (Tsun et al., 2013). To resolve this apparent discrepancy between genetic and biochemical data, we used the fission yeast FLCN homolog, Bhd1, as a model for TORC1 regulation.

In recent years, the fission yeast has emerged as a great model for studying the conserved aspects of amino acid-dependent regulation of TORC1. In this organism, the components of the TORC1 pathway are conserved (Alvarez and Moreno, 2006; Hayashi et al., 2007; Matsuo et al., 2007), including the TSC1-TSC2-Rheb signaling axis (Mach et al., 2000; Urano et al., 2005; Uritani et al., 2006), which is absent in *Saccharomyces cerevisiae* (Tatebe and Shiozaki, 2017; Urano et al., 2000). *S. cerevisiae* possesses an FLCN homolog called Lst7 (Péli-Gulli et al., 2015; Peli-Gulli et al., 2017) which physically interacts with a protein whose structure is orthologous to FNIP, Lst4 (Pacitto et al., 2015) and localizes to vacuoles – the yeast equivalent of lysosomes – in response to nitrogen starvation. This complex functions as a GAP for Gtr2 to activate TORC1 following nitrogen replenishment. Because of the absence of the TSC-Rheb signaling axis in *S. cerevisiae* and its prevalence in other eukaryotes, we reasoned that *S. pombe* represents a closer model for studying the conserved aspect of FLCN-mediated TORC1 regulation to other eukaryotes. Critically, *S. pombe* contains structural and functional orthologs of both heterodimeric Rag GTPases and their associated GEFs and GAPs. Gtr1-Gtr2 GTPase heterodimers are equivalent to the mammalian RagA/B and RagC/D (Nakashima et al., 1999). This dimer is recruited to the membranes of vacuoles through interaction with the tetrameric Lam protein complex (Lam1-Lam2-Lam3-Lam4) which is structurally related

to the mammalian Ragulator complex, and its Lam2 subunit possesses sequence similarity to the human Ragulator subunit, Lamtor2 (Chia et al., 2017). Moreover, the fission yeast has a GATOR1-like complex, which akin to its human counterpart (Bar-Peled et al., 2013), acts as a GAP on Gtr1 to regulate TORC1 activity in response to amino acid levels (Chia et al., 2017). Vam6, rather than Ragulator, has been identified as a GEF for Gtr1 with the GTP-bound form of Gtr1 interacting with TORC1 and being required for its amino acid-responsive activation (Binda et al., 2009; Valbuena et al., 2012a; Wurmser et al., 2000). Finally, Bhd1 has been identified as the FLCN homolog in fission yeast; however, an FNIP homolog has not been identified in this organism (van Slegtenhorst et al., 2007).

Here, we characterize the FLCN-FNIP complex in the fission yeast and show that this complex (the Bhd1-Fnp1 complex, or BFC), similar to its mammalian counterpart, acts as an activator of TORC1 upon amino acid stimulation. Additionally, we show that BFC augments TORC1 repression when cells are starved for amino acids. Specifically, we find that BFC mutant cells display slower kinetics of TORC1 repression and grow faster than wild-type cells after a short pulse of amino acid starvation. Interestingly, BFC physically associates with the V-ATPase complex and regulates its activity in an amino acid-dependent manner. Finally, by comparing the proteomic and genetic interaction networks of BFC, we identify Ptr2, a vacuolar amino acid transporter, and Ade3, a protein required for adenine biosynthesis, as two new proteins that also repress TORC1 activity in response to amino acid starvation. Taken together, these data ascribe a repressive function to BFC in TORC1 regulation and establish *S. pombe* as an excellent model for uncovering the molecular mechanisms by which FLCN represses TORC1 in response to amino acid starvation in eukaryotes.

RESULTS

Identification of the FNIP homolog in the fission yeast

FNIP1 and FNIP2 are interacting partners of FLCN in human cells (Hasumi et al., 2008; Takagi et al., 2008). To identify and characterize interacting partners of the fission yeast FLCN homolog Bhd1, we purified the native Bhd1 complex by constructing a strain in which the endogenous *bhd1* gene was fused in-frame with tandem affinity purification (*TAP*) at its C terminus, expressing the Bhd1-TAP fusion protein. Previously we showed that an auxotrophic strain (carrying a deletion of *bhd1*) display a growth advantage over wild-type strains on rapamycin-containing plates (Laviolette et al., 2017) (Figure S1A). By plating an equal number of log phase *bhd1-TAP*, *bhd1Δ* and wild-type cells in a 10-fold concentration gradient on rapamycin-containing plates, we found that the *bhd1-TAP* and wild-type strains grow with similar efficiencies in contrast to the *bhd1Δ* cells which displayed a growth advantage over wild-type (Figure S1B). These data suggest that the fusion protein is functional and behaves similar to the wild-type protein. Next, to define the native Bhd1 complex in *S. pombe*, we performed two independent Bhd1-TAP two-step affinity purifications along with parallel untagged control purifications. The purified proteins were analyzed by polyacrylamide gel electrophoresis and liquid chromatography-tandem mass spectrometry (LC-MS/MS) (Figure 1A). These data revealed that the purification of Bhd1-TAP co-immunoprecipitated a previously uncharacterized protein SPAC30C2.07 as the most abundant Bhd1-interacting protein (Figure 1B and Table S1). Similarly, two independent purifications of the functional (Figure S1B), C-terminally TAP-tagged SPAC30C2.07 protein (Figure 1A) yielded Bhd1 as its predominant interacting partner (Figure 1B and Table S2). These data demonstrate that Bhd1 and SPAC30C2.07 interact reciprocally, suggesting that SPAC30C2.07 may be the fission yeast ortholog of FNIP.

Sequence alignment between the SPAC30C2.07 and the human FNIP2 (hFNIP2) proteins revealed 29% identity between them (Figure S1C). To evaluate whether the two proteins share any conserved structural features, we extracted the hFNIP2 structure from the recently described cryo-EM structure of the human FLCN-FNIP2-Rag-Ragulator complex (PDB ID: 6ULG.N) (Shen et al., 2019). Modeling the SPAC30C2.07 based on the hFNIP2 structure, revealed that the secondary structure elements of the Longin and DENN domains of hFNIP2 are well conserved in SPAC30C2.07 (Figure S1C), including the split Longin domain characteristic of the FNIP family of proteins. The Longin domains of hFNIP2 and FLCN heterodimerize to form a ten-stranded β-sheet, surrounded by six α-helices (Shen et al., 2019). All secondary structure elements required for complex formation with FLCN appear to be conserved in the SPAC30C2.07 Longin domain. Likewise, the long α-helices at the C terminus of the hFNIP2 primary sequence (αD9 and αD10) that contribute to the interface for the heterodimerization of the hFNIP2 and FLCN DENN domains are also well conserved in the predicted SPAC30C2.07 structure (Figures 1C and 1D). Of note, the SPAC30C2.07 αD10 is disrupted by a short loop toward the C terminus. There are also a few other

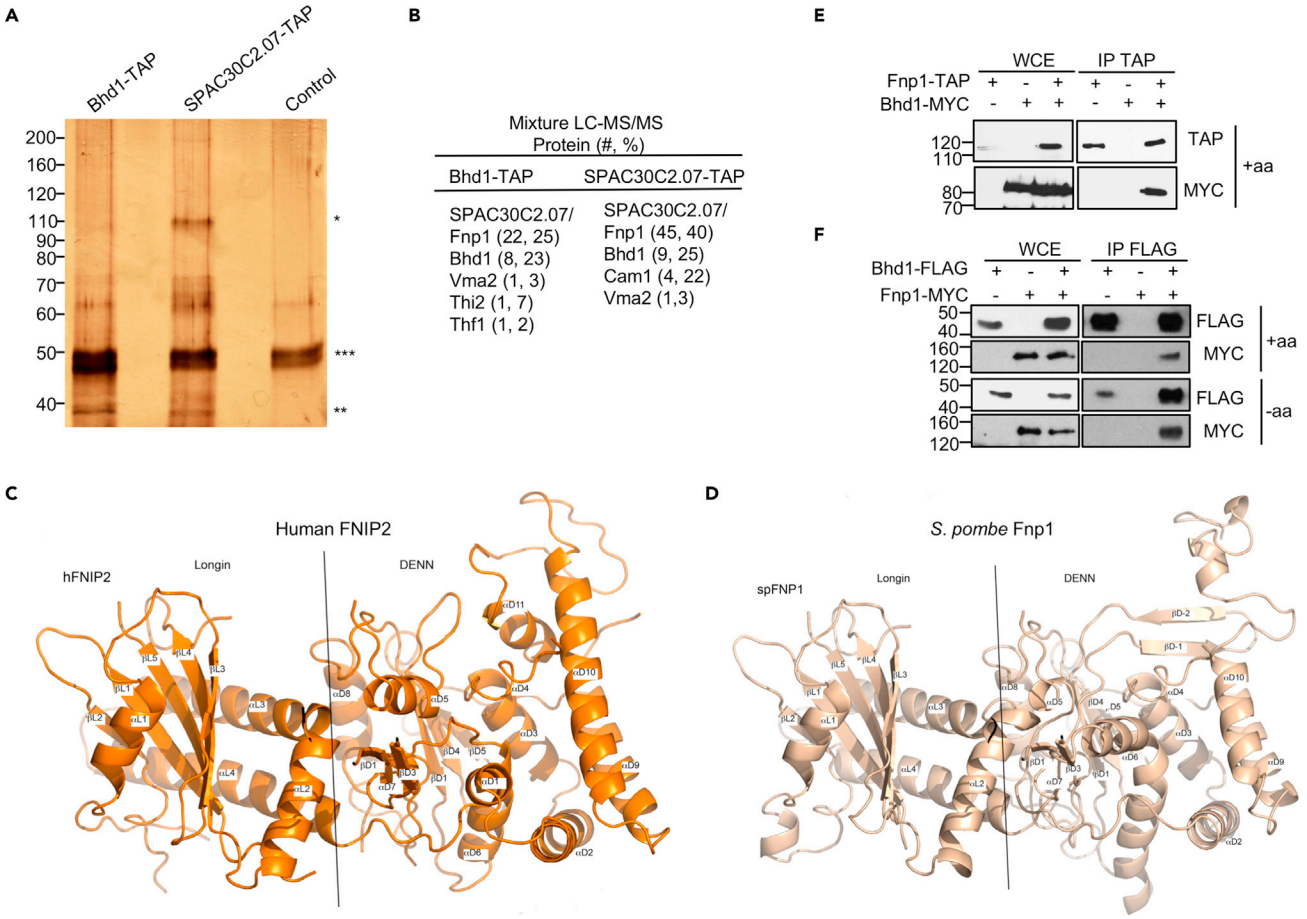

Figure 1. Purification and characterization of the *S. pombe*Bhd-FnpComplex (BFC)

(A) A representative silver-stained SDS-PAGE depicting the result of two-step tandem affinity purifications from *bhd1-TAP*, *SPAC30C2.07-TAP* (*fnp1-TAP*), and control (no TAP-tagged) strains. Two independent purifications were performed. Putative Fnp1 (*) and Bhd1 (**) proteins are denoted based on their theoretical mass of 93.38kDa and 40.8kDa, respectively. (***) denotes background protein common to all purifications.

(B) Proteins identified using tandem mass spectrometry sequencing (LC-MS/MS) which were unique to Bhd1-TAP or SPAC30C2.07-TAP (Fnp1-TAP) purifications after removing background (control purification) proteins. The numbers in parentheses correspond to the total number of peptides and percent protein coverage based on total number of amino acids, respectively, for one representative purification. See Tables S1 and S2.

(C) Cryo-EM structure of hFNIP2 extracted from the FLCN-FNIP2-Rag-Ragulator complex (PDB ID 6ULG.N). Longin and DENN domains and their respective secondary structure elements are highlighted.

(D) Structural model of the *S. pombe* Fnp1 based on the human FNIP2 structure. Domain boundaries and secondary structure elements are labeled using the human FNIP2 nomenclature.

(E) A representative Western blot depicting Fnp1-TAP immunoprecipitation co-precipitates Bhd1-MYC when cells are grown continuously in minimal media supplemented with amino acids. Three independent biological replicates were performed.

(F) A representative Western blot showing that Bhd1-FLAG immunoprecipitation co-precipitates Fnp1-MYC when cells are grown continuously in minimal media supplemented with amino acids (+aa) or are starved for amino acids for 90 min (-aa). Three independent biological replicates were performed. WCE, whole cell extract.

deviations between the structures. The first α-helix of the hFNIP2 Longin domain (αL1) which contacts the nucleotide binding domain of the RagC GTPase in the FLCN-FNIP2-Rag-Ragulator structure (Shen et al., 2019) is conserved on SPAC30C2.07. However, R72, which corresponds to R130 on hFNIP2, located just before αL1 is one amino acid closer to the helix, suggesting a slightly different mode of interaction with GTPases or other interaction partners (see sequence alignment in Figure S1C). Also, the first α-helix of the hFNIP2 DENN domain (αD1) is missing from the SPAC30C2.07 sequence and an extended loop between αD5 and βD1 of SPAC30C2.07 is predicted to accommodate a small β-sheet. We labeled the strands βD-2 and βD-1 to emphasize that these are hypothetical β-strands that are not present in the hFNIP2 structure. This sheet substitutes for αD11 in the SPAC30C2.07 structure. Overall, these analyses reveal that

SPAC30C2.07 has broad sequence and structural similarities to the members of the FNIP family of proteins, which together with the purification data demonstrate that SPAC30C2.07 is the ortholog of human FNIP proteins. We have named SPAC30C2.07 protein folliculin-interacting protein 1, or Fnp1.

Bhd1-Fnp1 complex (BFC) formation occurs independently of amino acid availability

To corroborate Bhd1-Fnp1 interaction, we performed reciprocal co-immunoprecipitation (co-IP) experiments using strains expressing endogenous *bhd1* and *fnp1* tagged with TAP, FLAG, or MYC epitopes at their C termini. Cells expressing the tagged proteins did not show any aberrant growth on rapamycin plates compared to wild-type cells (Figure S1B), suggesting that the tagged proteins are functional. As shown in Figure 1E, Fnp1-TAP immunoprecipitation co-precipitated Bhd1-MYC and, reciprocally, Bhd1-FLAG pull-down co-precipitated Fnp1-MYC (Figure 1F), indicating that Bhd1 and Fnp1 form a complex in the fission yeast. We call this complex the Bhd1-Fnp1 complex (BFC).

Previous studies have shown that interaction of FLCN-FNIP1/2 is insensitive to amino acid availability in human cells (Meng and Ferguson, 2018). To test whether the *S. pombe* BFC complex formation is also insensitive to amino acid levels, co-IP experiments using auxotrophic cells (*ade*$^{-}$, *ura*$^{-}$, *leu*$^{-}$) expressing Bhd1-FLAG, and Fnp1-MYC were performed with cells continuously grown in Edinburgh minimal media (EMM) with supplements (0.225 g/L adenine, histidine, leucine, lysine and uracil) (+aa) or starved for amino acids for 90 min without supplements (-aa). For this paper, the reasons that we used an auxotrophic strain instead of a prototrophic strain for amino acid regulation of TORC1 are: (1) considering this study focuses on the amino acid dependent regulation of TORC1, using an auxotroph which we can starve for amino acids would make our experiments consistent with the goal of our study; (2) extensive transcriptome and growth analyses of auxotrophic versus prototrophic strains by the David Botstein group in the budding yeast (*S. cerevisiae*) have revealed that auxotrophic strains grown on limited nutrient media waste excess sugar in a phenomenon that is both metabolically and transcriptionally similar to the Warburg Effect in cancer cells (Bruar, 2008). These suggest that auxotrophic strains are a better model for understanding the amino acid-dependent regulation of TORC1 within a cancer context; and (3) even though several other studies use nitrogen starvation as a surrogate for amino acid starvation, nitrogen starvation in the fission yeast not only induces the mating response (Engel, 2004) but its persistence also forces cells into quiescence in a two-step process which involves the early upregulation of mating genes followed by establishment of the quiescence transcriptome (Joh et al., 2016; Marguerat et al., 2012; Shimanuki et al., 2007). To avoid the complex biology associated with nitrogen starvation and considering our focus is amino acid-dependent regulation of TORC1 by FLCN, we reasoned that using amino acid starved auxotrophs is justified for this study. Similarly, other papers (for example (Chia et al., 2017; Fukuda et al., 2021; Valbuena et al., 2012a; Valbuena et al., 2012b)) also employ auxotrophs for studying amino acid-dependent regulation of TORC1 in *S. pombe*. Using the above-mentioned strains, we found that FLAG-tagged Bhd1 co-precipitated Fnp1-MYC under both starved and amino acid replete states (Figure 1F). These data demonstrate that, consistent with the mammalian FLCN/FNIP complex, the *S. pombe* BFC formation is amino acid independent.

BFC localizes to vacuoles in response to amino acid starvation

The mammalian FLCN-FNIP complex translocates to the lysosomal surface in response to amino acid starvation (Meng and Ferguson, 2018; Tsun et al., 2013). To determine whether the BFC also localizes to vacuolar membranes in response to amino acid starvation in the fission yeast, we used the lipophilic styryl dye FM4-64 as marker for visualizing vacuolar membranes. As a positive control, we tagged the vacuolar-membrane associated small GTPase Ypt7, a homolog of the human late endosome/lysosome small GTPase Rab7, with GFP (Price et al., 2000). Consistent with previous reports (Brazer et al., 2000; Iwaki et al., 2003, 2004; Vida and Emr, 1995), we found a nearly complete overlap between the FM4-64 and GFP-tagged Ypt7 fluorescence signals, confirming FM4-64 as a vacuolar membrane-specific dye (Figures S2A and S2B). Moreover, in contrast to the functionally antagonistic Rab7 homologs Ypt7 and Ypt71, whose deletions result in smaller and larger vacuoles compared to wild-type, respectively (Kashiwazaki et al., 2009), we found that deletion of *bhd1* and *fnp1* did not result in any observable vacuolar size alterations (Figure S2C).

Next, to visualize BFC, we constructed strains expressing C-terminally GFP-tagged Bhd1 and Fnp1 proteins from their endogenous promoters. We found that the expression of the GFP tagged version of these proteins is not impacted by 90 min of amino acid starvation (Figure S2D). Live-cell fluorescence microscopy revealed that both Bhd1 and Fnp1 appear diffusely distributed throughout the cytoplasm in amino acid-

replete conditions, but localize to vacuoles in response to amino acid starvation evidenced by the strong overlap between Bhd1-/Fnp1-GFP and the FM4-64 dye under amino acid starvation conditions (Figures 2A–2F). Also, to determine whether vacuolar localization of Bhd1 depends on Fnp1 or vice versa, we constructed *fnp1Δ bhd1-GFP* and *bhd1Δ fnp1-GFP* strains. Live-cell fluorescence microscopy revealed that the recruitment of Bhd1 and Fnp1 to vacuoles is only partially dependent on the other protein (Figure S3). Together these data demonstrate that Bhd1 and Fnp1 localize to vacuoles in response to amino acid starvation and that this localization is largely independent of the presence of the other protein.

BFC augments TORC1 activation in response to amino acid stimulation

Previous studies have shown that the mammalian FLCN/FNIP complex activates the mTORC1 signaling pathway following amino acid stimulation (Nookala et al., 2012; Petit et al., 2013; Tsun et al., 2013). To determine whether the fission yeast BFC similarly activates TORC1 in response to amino acid stimulation, wild-type, *fnp1Δ* and *bhd1Δ* cultures were grown continuously in EMM plus amino acids until log phase and then starved for amino acids for 140 min. This is a time point at which no Rps6 phosphorylation, a surrogate for TORC1 activity in eukaryotes (Nakashima et al., 2010), is detected in wild-type or BFC mutant cells (Figure 2G). For these experiments, Rps6 phosphorylation levels were monitored at regular intervals following amino acid supplementation. In all Western blots, because we were unable to find a commercial source for an antibody against total Rps6 protein, we used tubulin or actin as loading controls. These data revealed that TORC1 reactivation is delayed by 1–1.5 h in *fnp1Δ* and *bhd1Δ* cultures compared to wild type (Figures 2G and S4), demonstrating that the BFC, similar to the mammalian FLCN/FNIP complex (Petit et al., 2013; Tsun et al., 2013), is required for efficient activation of TORC1 following amino acid supplementation.

BFC enhances TORC1 repression in response to amino acid starvation

So far, our data demonstrate that amino acid-dependent regulation of BFC mimics its mammalian counterpart, suggesting a suitable model for studying FLCN functions in eukaryotes. Previous work in BHD patients (Vocke et al., 2005), FLCN-null mice (Baba et al., 2008; Chen et al., 2008; Hasumi et al., 2009; Wu et al., 2015), and *S. pombe bhd1Δ* strain (Laviolette et al., 2017) suggest that FLCN also may repress TORC1 activity under certain physiological conditions. To ask whether loss of BFC impacts steady-state growth, we first measured the growth rate of wild-type and BFC mutant strains grown continuously in EMM supplemented with amino acids and found that *bhd1Δ* and *fnp1Δ* mutant strains grow at a similar rate to wild type cells (Figures S5A and S5B).

Previously, we showed that loss of Bhd1 in auxotrophic strains (*leu*$^-$, *ade*$^-$, *ura*$^-$) results in increased Rps6 phosphorylation when cells are deprived of amino acids (supplemented with 5-fold lower amino acid concentration than standard media) (Laviolette et al., 2017), suggesting that Bhd1 may help repress TORC1. Consistent with a repressive role for BFC on TORC1 activity, here, we also found that deletion of BFC (*bhd1* or *fnp1*) results in a significant growth advantage of BFC mutant over wild-type strains when equal number of log phase cells are grown on rapamycin-containing EMM plates supplemented with amino acids (Figures S1A and S1B). Moreover, treating cells with 125 or 150 ng/mL of rapamycin for 90 min revealed that the growth advantage of BFC mutants correlates with an increase in P-Rps6 levels compared to wild-type cells (Figure S5C). Together, these data support a model in which BFC participates in TORC1 repression.

Despite a potential role for BFC in TORC1 repression (Figures S1A and S1B), as shown in Figure 2G, after 140 min of amino acid starvation, no P-Rps6 could be detected in wild-type and BFC mutant cells, demonstrating that TORC1 repression can still occur in the absence of BFC. Based on these data, we hypothesized that BFC, in addition to its role in augmenting TORC1 activation in response to amino acid stimulation, may be required for the rapid repression of TORC1 in response to amino acid starvation. To test this hypothesis, we performed a timecourse starvation assay in which Rps6 phosphorylation levels were monitored in log-phase wild-type, *bhd1Δ* and *fnp1Δ* strains which were grown in EMM supplemented with amino acids and then starved for amino acids for 50, 70, or 90 min. Interestingly, we found that cells lacking either Bhd1 or Fnp1 proteins displayed slower kinetics of TORC1 repression compared to wild-type cells (Figure 3A), especially at 90 min when no detectable P-Rps6 could be observed in wild-type cells in contrast to *fnp1Δ* and *bhd1Δ* strains where a P-Rps6 signal is visible (Figure 3B). Previous work had shown that the availability of ammonium as a nitrogen source causes nitrogen catabolite repression in yeasts and filamentous fungi (Wiame et al., 1985) and can regulate TORC1 activity in metazoans (Merhi et al., 2017). To ask whether the BFC-mediated TORC1 repression requires the presence of ammonium, we used Pombe minimal glutamate medium (PMG) in which ammonium chloride is replaced by glutamic acid as the sole

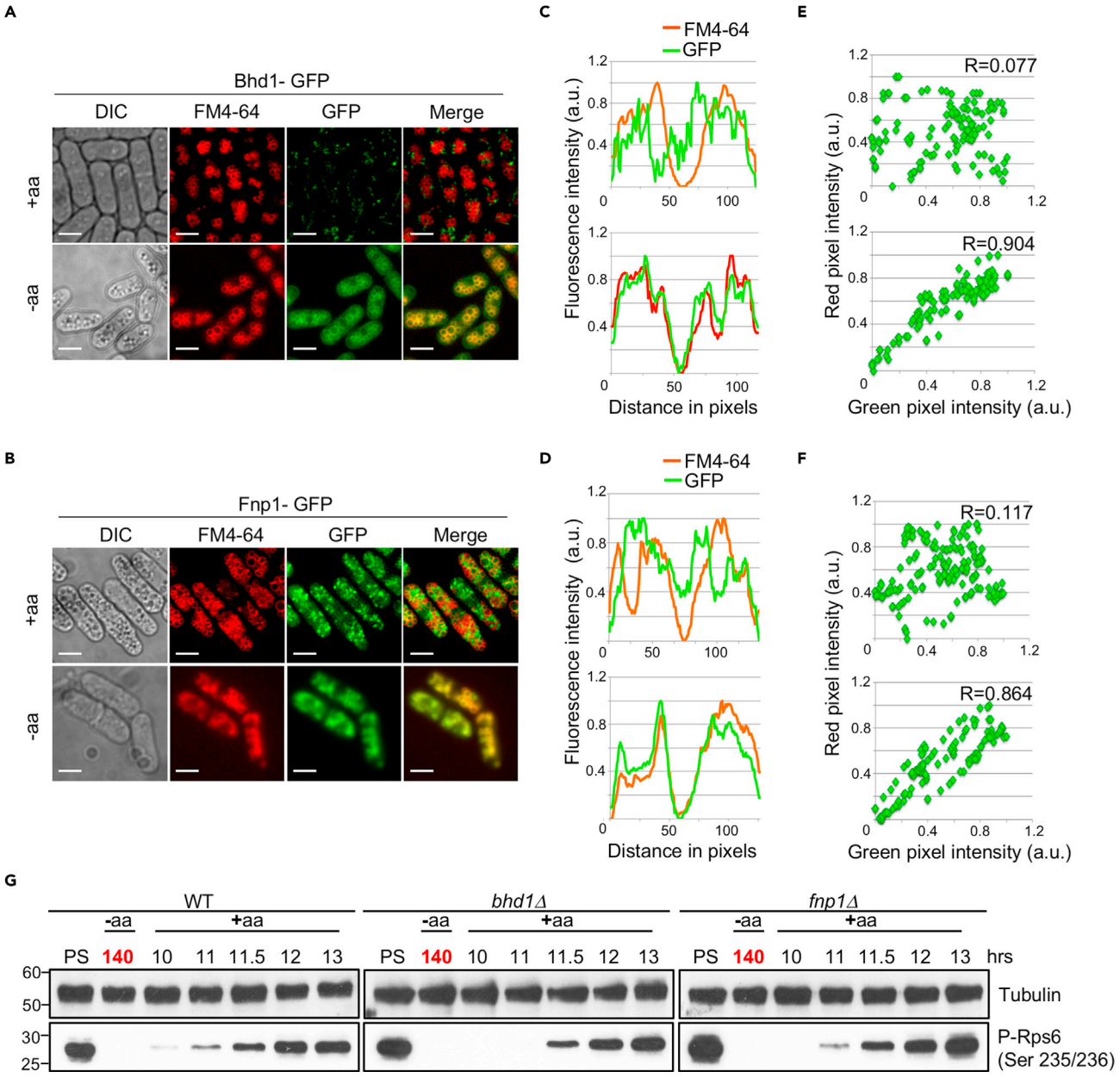

Figure 2. BFC localizes to vacuoles in response to amino acid starvation and augments TORC1 activation in response to amino acid stimulation

Representative fluorescence microscopy images depicting the co-localization of (A) Bhd1-GFP and (B) Fnp1-GFP with vacuoles (FM4-64-Red) for cells grown continuously in minimal media supplemented with amino acids (+aa) or starved for amino acids for 90 min (-aa). Graphs depicting the fluorescent intensity signal of Bhd1-GFP (C) and Fnp1-GFP (D) along with FM4-64 after drawing a line from one end of the cell to another. Representative graphs used to calculate the Pearson correlation coefficient (R) of overlap between Bhd1-GFP (E) and Fnp1-GFP (F) with FM4-64. DIC - differential interference contrast; au.–arbitrary units; GFP – green fluorescent protein. 15 cells per replicate were analyzed for calculating R using ImageJ software. Three biological replicates were performed. See also Figures S2 and S3. Scale bar – 10μm.

(G) A representative Western blot depicting the kinetics of Rps6 phosphorylation (P-Rps6) after amino acid supplementation. Log phase wild-type (*WT*), *bhd1Δ* and *fnp1Δ* cells were starved for amino acids (-aa) for 140 min (red text), and then incubated in pre-warmed EMM supplemented with amino acids (+aa) for the indicated times (in hours). Because we were unable to find a commercial antibody for detecting total Rps6 levels, similar to previous studies (Chica et al., 2016; Ma et al., 2013; Martin et al., 2017; Matsuda et al., 2020; Nakashima et al., 2010; Nakashima and Tamanoi, 2010; Rodland et al., 2014; Valbuena et al., 2012a, 2012b), tubulin or actin were used as loading controls for Western blot analyses. Three biological replicates were performed. PS – pre-starvation.

See also Figure S4 for two other replicates.

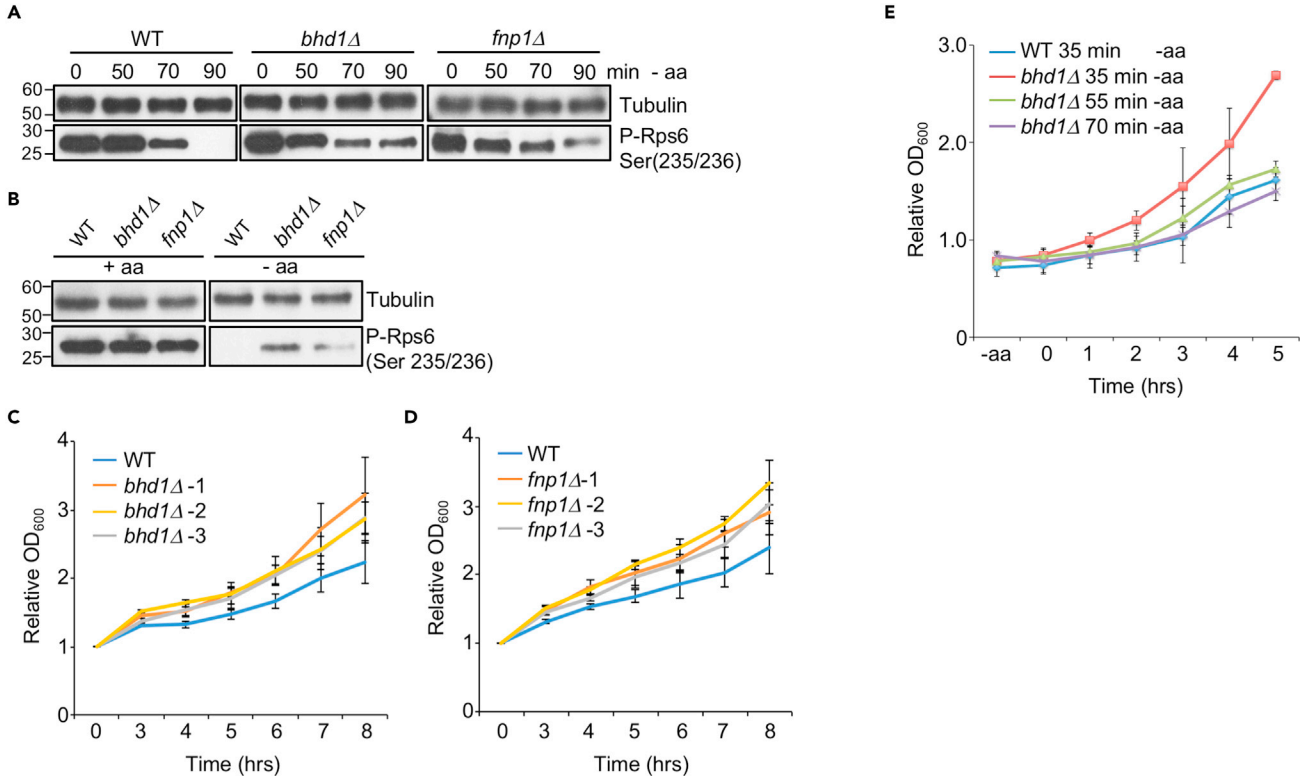

Figure 3. BFC augments TORC1 repression in response to amino acid starvation

(A) A representative Western blot depicting changes in P-Rps6 levels (P-Rps6 serine 235/236), a TORC1 substrate, using a specific P-Rps6 antibody in cells starved for amino acids (-aa) in wild-type (*WT*), *bhd1Δ* and *fnp1Δ* cells at the indicated time points (minutes) after amino acid starvation (-aa). Tubulin was used as a loading control. Three biological replicates were performed.

(B) A representative Western blot depicting P-Rps6 levels after 90 min of amino acid starvation. Tubulin was used as a loading control. Three biological replicates were performed. See also Figures S5D and S5E.

Graphs depicting the growth of WT and three independent *bhd1Δ* (C) or *fnp1Δ* (D) clones after a 25-min pulse of amino acid starvation. The measurements were taken starting at an OD600 between 0.25 and 0.3. Relative OD600 values (normalized to OD600 at t = 0) are plotted versus time (hours). Mean and standard deviation of three biological replicates are depicted.

(E) Graph depicting the growth of *WT* and *bhd1Δ* cells after different periods of amino acid starvation. The measurements were taken every hour starting at an OD600 between 0.25 and 0.3. Relative OD600 values (normalized to OD600 at t = 0) are plotted versus time (hours). Mean and standard deviation of three biological replicates are depicted.

nitrogen source. Consistent with our results in EMM, we found that cells lacking the Bhd1 protein displayed slower kinetics of TORC1 repression compared to wild-type cells (Figures S5D and S5E). Taken together, these data demonstrate that Bhd1 and Fnp1 are required for the rapid repression of TORC1 in response to amino acid starvation.

BFC mutants display a significant growth advantage over wild-type cells after a pulse of amino acid starvation

To ask whether the delay in TORC1 repression in BFC mutants in response to a short pulse of amino acid starvation has any functional consequences—for example, providing the mutant cells with a growth advantage over wild type—three independent clones of *bhd1Δ* and *fnp1Δ* were constructed (Table S8). These clones along with a wild-type control were grown continuously to log phase in EMM supplemented with amino acids and then starved for amino acids for 25 min after which amino acids were added to the media. Growth was then monitored hourly for 8 h after supplementation. Strikingly, we found that all three independent *bhd1Δ* and *fnp1Δ* clones displayed markedly faster growth compared to wild type (Figures 3C and 3D). In fact, we found that *bhd1Δ* cells starved for amino acids for 55 min display growth kinetics and, thus, a delay in TORC1 reactivation similar to wild-type cells starved for amino acids for 35 min (Figure 3E).

Collectively, these results demonstrate that BFC mutants are defective in rapid repression of TORC1, and thus have a growth advantage over wild-type cells following a short pulse of amino acid starvation.

BFC interacts with Vma2 subunit of the V-ATPase complex and regulates its activity in an amino acid-dependent manner

Two-step TAP purification of Bhd1-TAP helped identifyFnp1 as the predominant Bhd1 interacting protein. For characterizing this complex, we also performed additional one- and two-step TAP purifications of Bhd1-TAP and Fnp1-TAP. Unexpectedly, all one-step Bhd1 purifications also yielded the coimmunoprecipitation of other components of the V-ATPase complex (Vph1, Vma4, Vma5, Vma6, Vma8, Vma13) consistent with a physical interaction between BFC and V-ATPase complex (Tables S1 and S2). Specifically, Vma2, a 56kDa protein that functions as the regulatory subunit of the V1 cytoplasmic domain of the vacuolar-type H + ATPase (V-ATPase), was found as a BFC-interacting protein in all one- and several of the two-step Bhd1-TAP or Fnp1-TAP purifications (Figure 4A). Together, these data suggest that Vma2 interacts with BFC.

To confirm the physical interaction between Vma2 and BFC, we immunoprecipitated Bhd1-TAP and found that it co-precipitated Vma2-MYC in both amino acid replete and starved conditions (Figure 4B). Even though the co-immunoprecipitation experiments were not performed reciprocally, these data suggest that Bhd1 interacts with Vma2. To test the evolutionary conservation of the BFC-Vma2 interaction, we performed immunoprecipitation of TAP-tagged Lst7, the FLCN ortholog in *S. cerevisiae*, and probed its interaction with Vma2 in the presence of amino acids or when cells are starved for amino acids for 90 min by immunoblotting using an anti-Vma2 antibody. Similar to *S. pombe*, immunoblot results showed that the *S. cerevisiae* Lst7 immunoprecipitated Vma2-MYC in the presence or absence of amino acids (Figure 4C). Also, mass spectrometric analyses of one-step Lst7-TAP purification in addition to Lst4, the *S. cerevisiae* ortholog of FNIP, revealed the coimmunoprecipitation of Vma2 and other V-ATPase components (VPH1, VMA5, VMA6, VMA7, VMA8, VMA13) in *S. cerevisiae* (Table S3). Together these data suggest that Lst7 interacts with Vma2 in *S. cerevisiae*.

Vma2 interaction with the BFC prompted us to examine whether BFC regulates V-ATPase activity. A highly conserved function of the V-ATPase complex is to acidify vacuoles and lysosomes in organisms ranging from yeast to human. We therefore assayed vacuolar pH as a surrogate for V-ATPase activity, with alkalinization indicating reduced activity. The pH status of the vacuoles in wild-type, *bhd1Δ*, and *fnp1Δ* strains was visualized using DND189, a membrane-permeant weakly basic dye that fluoresces in acidic, but not alkaline compartments (Perzov et al., 2002). As a positive control, we also treated wild-type cells with 10nM bafilomycin, a specific V-ATPase inhibitor. We observed that the fluorescence intensity of DND189 is significantly reduced in *bhd1Δ* and *fnp1Δ* strains compared to wild-type cells and similar to wild-type cells treated with bafilomycin, suggesting that V-ATPase activity is reduced in the BFC mutant cells (Figure 4D). Quantitation of DND189 and FM4-64 fluorescence intensity confirmed a reduction in DND189, but not FM4-64 intensity in the deletion mutants (Figure 4E). Also, we found that the BFC-mediated V-ATPase regulation depends on the presence of amino acids (Figure S6). Previous studies have shown that disruption of V-ATPase activity affects cell growth on alkaline (pH = 9.0) plates in *S. pombe* (Iwaki et al., 2004). By plating an equal number of log phase *bhd1Δ*, *fnp1Δ* and wild-type cells in a 10-fold concentration gradient on pH 9.0 plates, we found that the BFC mutant strains grow less efficiently compared to the wild-type strain (Figure 4F). Similarly, we found that *bhd1Δ* and *fnp1Δ* cells grow less efficiently than wild-type cells when plated in the presence of bafilomycin, a specific inhibitor of V-ATPase (Figure 4F). Together, these data suggest that BFC physically interacts with the V-ATPase complex and regulates its activity in an amino acid-dependent manner.

Ptr2 and Ade3 enhance TORC1 repression in response to amino acid starvation

As mentioned previously, in addition to two-step Bhd1-TAP and Fnp1-TAP purifications, we also performed several one-step Bhd1-TAP and Fnp1-TAP purifications followed by mass spectrometric analysis. The one-step purifications permit the identification of sub-stoichiometric protein interactors and complexes which often function within the same pathway (Li, 2011). These data (Figure 5A;Tables S1 and S2) along with the pombe genetic interaction network (Table S7), useful for identifying proteins that operate within the same pathway (Ryan et al., 2012), revealed several nodes of physical and genetic interactions with BFC components, suggesting the involvement of these proteins and associated complexes in amino acid-dependent repression of TORC1 in *S. pombe*. Two proteins which interact with BFC both physically and genetically are

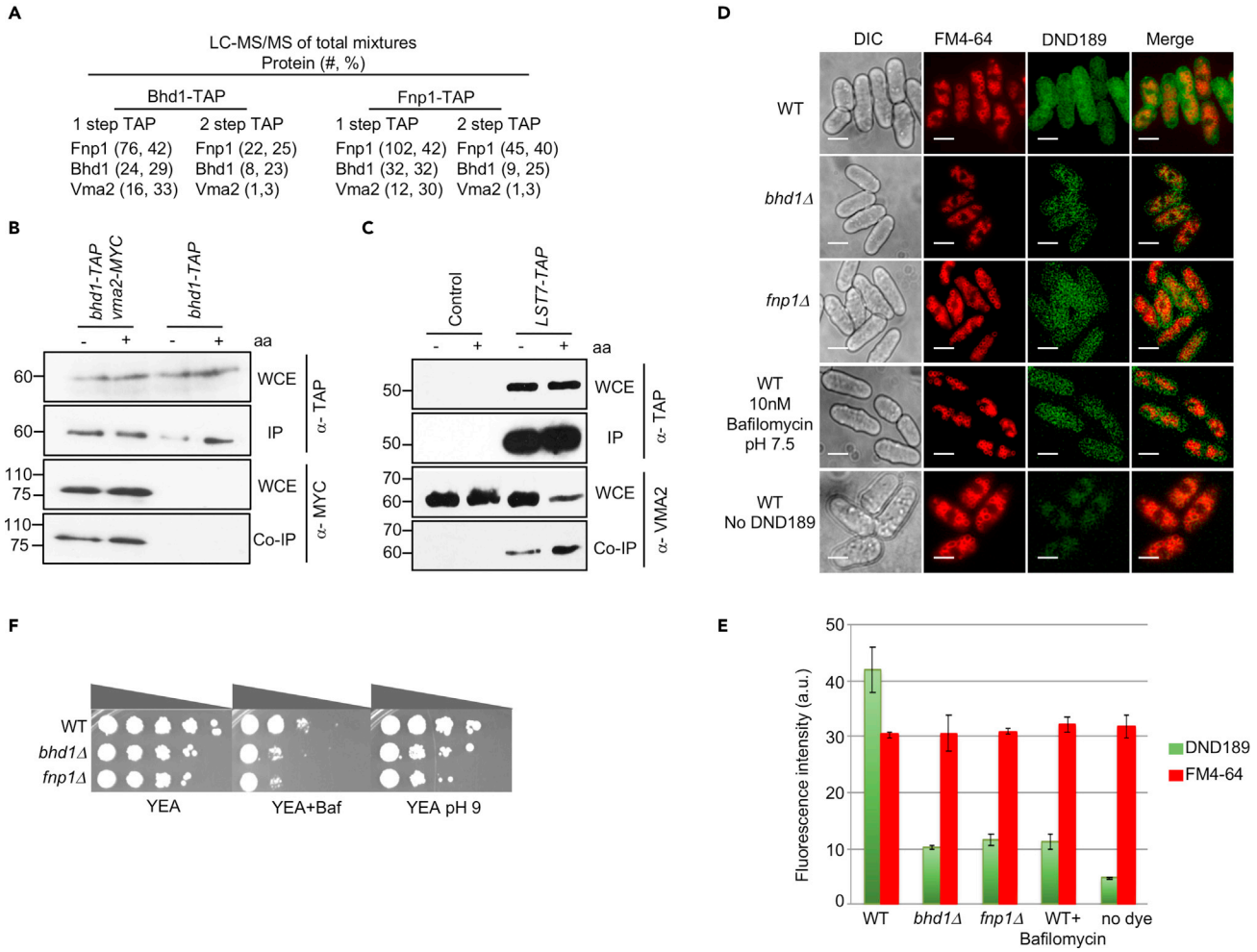

Figure 4. Bhd1 immunoprecipitates Vma2, a component of the V-ATPase complex, in *S. pombe* and *S. cerevisiae* and regulate its activity

(A) Tables listing proteins common to one-step Bhd1-TAP (n = 2), two-step Bhd1-TAP (n = 2), one step Fnp1-TAP (n = 5) and two-step Fnp1-TAP (n = 2) purifications. The numbers in parentheses correspond to the total number peptides and percent protein coverage based on total number of amino acids, respectively, for representative purifications. See also Tables S1 and S2.

(B) A representative Western blot showing that Bhd1-TAP co-precipitates with Vma2-MYC in presence (+aa) or absence (-aa) of amino acids. The images are representative of three biological replicates.

(C) A representative Western blot showing that Lst7-TAP (the *S. cerevisiae* homolog of Bhd1) co-precipitates Vma2 in presence (+aa) or absence (-aa) of amino acids. The images are representative of two biological replicates. Untagged *S. cerevisiae* cells were used as a negative control.

(D) Representative fluorescence microscopy images depicting vacuolar pH of *WT*, *bhd1Δ* and *fnp1Δ* cells grown continuously in EMM media supplemented with amino acids. FM4-64 (red) was used to stain vacuoles; DND189 (green) stains acidic organelles, such as vacuoles (pKa ~5.2). A culture of *WT* cells incubated with 10nM of Bafilomycin (V-ATPase-specific inhibitor) in pH 7.5 was used as positive control. Co-localization of green (acidic pH) and red (vacuole) pixels is depicted (Merge). DIC - differential interference contrast. Scale bar – 10μm.

(E) Graph representing the quantification of co-localization of red (vacuoles) and green (acidic organelles) pixels. Mean and standard deviation of three independent experiments are shown. See also Figure S6.

(F) Indicated strains were grown to log phase in complete media (YEA) and then spotted in 10-fold decreasing serial dilutions on YEA, YEA plus 700nM Bafilomycin and YEA pH = 9.0.

Ptr2 and Ade3 (Tables S1 and S2). Interestingly, in *S. cerevisiae*, Ptr2 and Ade3 homologs (called Ptr2 and Ade6) also coimmunoprecipitated with Lst7-TAP (Table S3), suggesting that these interactions are also conserved in the distantly related budding yeast. Ptr2 is the proton-coupled di- or tri-peptide transporter family member in *S. pombe* (also called peptide transporter (PTR) or SLC15 family), required for transport of dipeptides in this organism (Kitamura et al., 2017). Ade3 is a conserved protein with phosphoribosylformyl-glycinamidine synthase activity whose only known function is in adenine biosynthesis. In addition to Ade3, we found several other adenine biosynthetic genes in our Fnp1-and Bhd1-TAP one-step purifications, with

A

LC-MS/MS of total mixtures
Protein (#, %)

Expt 1		Expt 2	
Bhd1-TAP	Fnp1-TAP*	Bhd1-TAP	Fnp1-TAP*
Ptr2 (9, **)	Ptr2 (5, 11)	Ptr2 (8, 17)	Ptr2 (5, 10)
Ade3 (2, **)	Ade3 (16, 11)	Ade3 (10, 11)	Ade3 (15, 15)

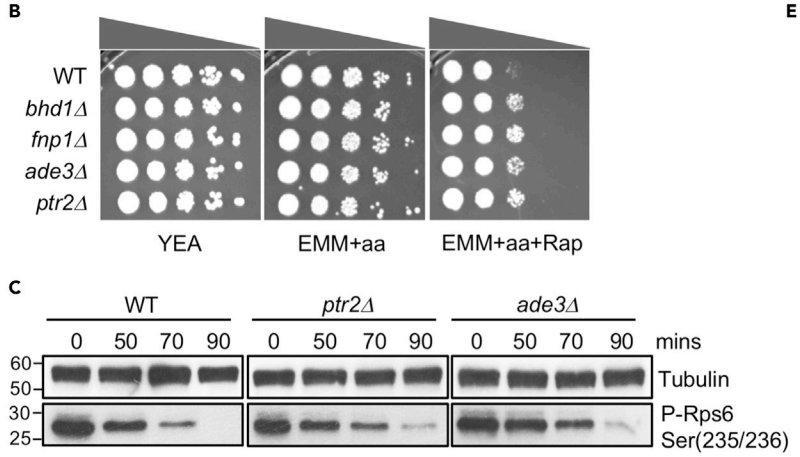

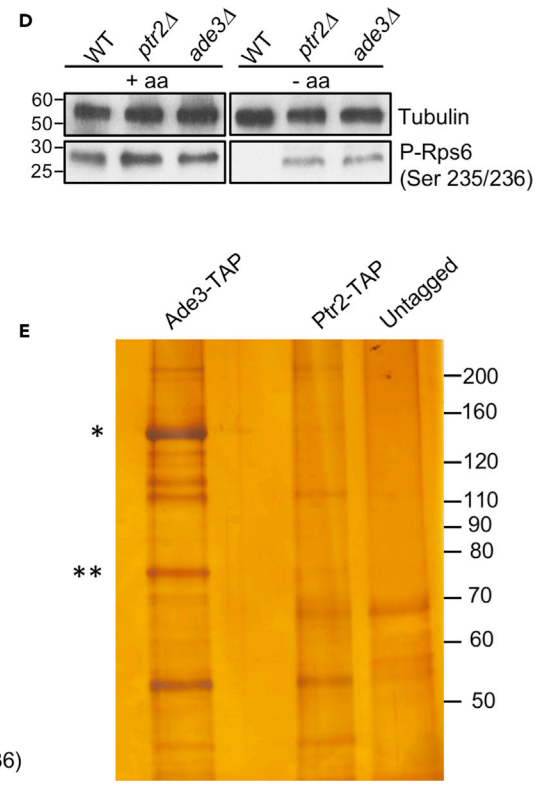

Figure 5. Ptr2 and Ade3 participate in amino acid dependent repression of TORC1

(A) Table indicating the total number of Ptr2 and Ade3 peptides identified in tandem mass spectrometry sequencing (LC-MS/MS) of Bhd1-TAP and Fnp1-TAP purifications. The numbers in parentheses correspond to total number of peptides and percent protein coverage based on total number of amino acids, respectively, from two representative one-step purifications. *Five independent one-step Fnp1-TAP purifications were performed; the data presented are representative of two such purifications. **Percent protein coverage was not available for this purification. See Tables S1 and S2.

(B) *ade3Δ* and *ptr2Δ* display a growth advantage over wild-type (*WT*) strain when grown on rapamycin-containing plates similar to *bhd1Δ* and *fnp1Δ* strains. Indicated strains were grown to log phase in minimal media plus amino acids (EMM + aa) media and then spotted in 10-fold decreasing serial dilutions on complete (YEA), synthetic minimal media supplemented with amino acids (0.225 g/L adenine, histidine, leucine, lysine and uracil) (EMM + aa) or on EMM + aa with rapamycin (EMM + aa + Rap) plates.[Rapamycin] = 200ng/mL.

(C) A representative Western blot depicting the kinetics of P-Rps6 downregulation in wild-type (*WT*), *ptr2Δ* and *ade3Δ* cells at the indicated time points (minutes) after amino acid starvation. Tubulin was used as a loading control. Three biological replicates were performed.

(D) A representative Western blot depicting the phosphorylation level of Rps6 (P-Rps6 serine 235/236), a TORC1 substrate, using a specific P-Rps6 antibody in *ptr2Δ* and *ade3Δ* mutant cells starved for amino acids (-aa) for 90 min. *WT* used as a control. Tubulin is used as the protein loading control. Three biological replicates were performed.

(E) A representative silver-stained SDS-PAGE depicting the result of two-step tandem affinity purifications from *ade3-TAP*, *ptr2-TAP*, and control (untagged) strains. Putative Ade3 (*) and Ptr2 (**) proteins are denoted based on their theoretical mass of 144.87 kDa and 68.5kDa, respectively.

See also Tables S5 and S6.

purine biosynthesis as one of the common gene ontology terms enriched in our datasets (Tables S1 and S2). Moreover, by examining the previously published purification of FLCN from mammalian cells (Laviolette et al., 2017), we found that GART, the mammalian homolog of Ade1/Ade5 co-immunoprecipitated with FLCN (Table S4), suggesting FLCN interaction with adenine biosynthesis proteins spans yeast to human cells. In fact, we found that 77 proteins which co-immunoprecipitated with Bhd1-TAP and Fnp1-TAP in the fission yeast have a human homolog which also co-immunoprecipiated with the human FLCN (Laviolette et al., 2017). These data together suggest that the *S. pombe* BFC can serve as an excellent model for understanding FLCN-regulated mechanisms in eukaryotes.

To test whether Ptr2 and Ade3 similar to the BFC are also involved in TORC1 regulation, we plated an equal number of log-phase *ade3Δ*, *ptr2Δ*, BFC-mutant and wild-type cells in a 10-fold concentration gradient on rapamycin-containing plates and found that similar to BFC mutants, *ade3Δ* and *ptr2Δ* strains grow more efficiently than wild-type (Figure 5B). Next, to ask whether these proteins are required for efficient

repression of TORC1 in response to amino acid starvation, we assayed TORC1 activity in response to amino acid starvation in *ptr2Δ* and *ade3Δ* strains. Our results revealed that similar to BFC, Ade3, and Ptr2 are required for efficient repression of TORC1 in response to amino acid starvation (Figures 5C and 5D). We also created C-terminally TAP tagged Ptr2-TAP and Ade3-TAP fusion proteins and purified these proteins using a one- and two-step TAP purification schemes (Figure 5E). We found that Ptr2 immunoprecipitation not only coimmunoprecipitated V-ATPase components (Vph1, Vma6, Vma2), but also several ion (Pho84, Pmc1, Zrt1, Fip1) and amino acid (Aat1, Cat1, Per1) transporters (Table S5). Ade3 on the other hand primarily co-immunoprecipitated 19S and 20S proteasome components as well as purine and amino acid biosynthetic proteins (Table S6). Together, these data demonstrate that Ptr2 and Ade3 interact with a network of transporters and biosynthetic proteins, respectively, and participate in the amino acid dependent repression of TORC1 in the fission yeast.

BFC localizes to vacuoles in response to amino acid starvation. Similarly, we found that Ade3-GFP is diffuse in amino acid replete conditions and localizes to vacuoles when cells are starved of amino acids for 90 min (Figure 6A). On the other hand, in contrast to BFC and Ade3, Ptr2-GFP localization clearly overlaps with vacuoles under both amino acid replete and starved conditions, demonstrating that Ptr2 localization to vacuoles is amino acid independent (Figure 6B). Interestingly, we also found that in *ptr2Δ* cells both Bhd1 and Fnp1 localize to vacuoles in amino acid replete conditions, which is only modestly augmented upon amino acid starvation (compare BFC localization in Figure S7 versus Figure 2). Overall, these data demonstrate that Ptr2 and Ade3 also regulate TORC1 activity in an amino acid-dependent manner.

DISCUSSION

BFC, an amino acid-dependent regulator of TORC1

In this study, the biochemical purification of the *S. pombe* FLCN homolog, Bhd1, identified SPAC30C2.07 protein (which we called Fnp1) as the FNIP family ortholog in this organism (Figures 1C, 1D, and S1C). Sequence alignment and homology-based structural modeling revealed that Fnp1 possesses an N-terminal Longin and a C- terminal DENN domain similar to the human FNIP protein. This complex (Bhd1-Fnp1 complex, or BFC), similar to the mammalian FLCN-FNIP, localizes to vacuoles in response to amino acid starvation and is required for efficient activation of TORC1 in response to amino acid supplementation (Figures 2,S3, and S4). The functional and structural conservation between BFC and FLCN-FNIP suggested that BFC could serve as a suitable model for exploring the functional role of this complex in TORC1 regulation. In support of this, we also found that by comparing our BFC versus FLCN (Laviolette et al., 2017) purifications, we found 77 BFC-interacting proteins whose homolog also co-immunoprecipitated with FLCN in human cells (Table S4). These data suggest that FLCN protein interaction network is conserved from yeast to human cells.

Previous work on BHD patients revealed that FLCN is a tumor suppressor protein (Hudon et al., 2010; Khoo et al., 2003; Warren et al., 2004) with the second loss-of-function mutation in this gene preceding RCC development in these patients (Vocke et al., 2005). Moreover, conditional kidney-specific knockout of *FLCN* in mice results in larger polycystic kidneys, an increased risk of RCC and higher TORC1 activity (Baba et al., 2008; Chen et al., 2008; Hasumi et al., 2009; Wu et al., 2015). These results suggest that in mammals FLCN's tumor suppressor activity may be through TORC1 repression. However, biochemical and cell culture studies have demonstrated that FLCN is required for activation of TORC1 in mammals (Petit et al., 2013; Tsun et al., 2013).

Considering the similarity between FLCN-FNIP and BFC complexes, we used *S. pombe* BFC to ask whether this complex could also function to repress TORC1 in this organism. Previously, we found that loss of Bhd1 in auxotrophic strains (*leu*$^-$, *ade*$^-$, *ura*$^-$) results in (1) increased TORC1 activity when cells are deprived of amino acids, and (2) increased cell growth in mutant strains compared to wild type when cells are grown on rapamycin-containing media (Laviolette et al., 2017), suggesting a repressive role for Bhd1 in TORC1 regulation. Accordingly, here we found that BFC is required for the efficient repression of TORC1 in response to amino acid starvation (Figures 3 andS5C–S5E) and rapamycin treatment (Figures S1A, S1B, and S5C). In fact, a short pulse of amino acid starvation provides BFC-mutant cells with a growth advantage over wild-type cells (Figures 3C–3E). These data together suggest that in *S. pombe* BFC can act as a switch or rheostat, toggling TORC1 activity off or on in response to amino acid availability and the physiological state of the cell. Considering the conservation of BFC and FLCN-FNIP complexes, these data also raise the possibility that in mammals, loss of FLCN may result in context-dependent defects in mTOR regulation

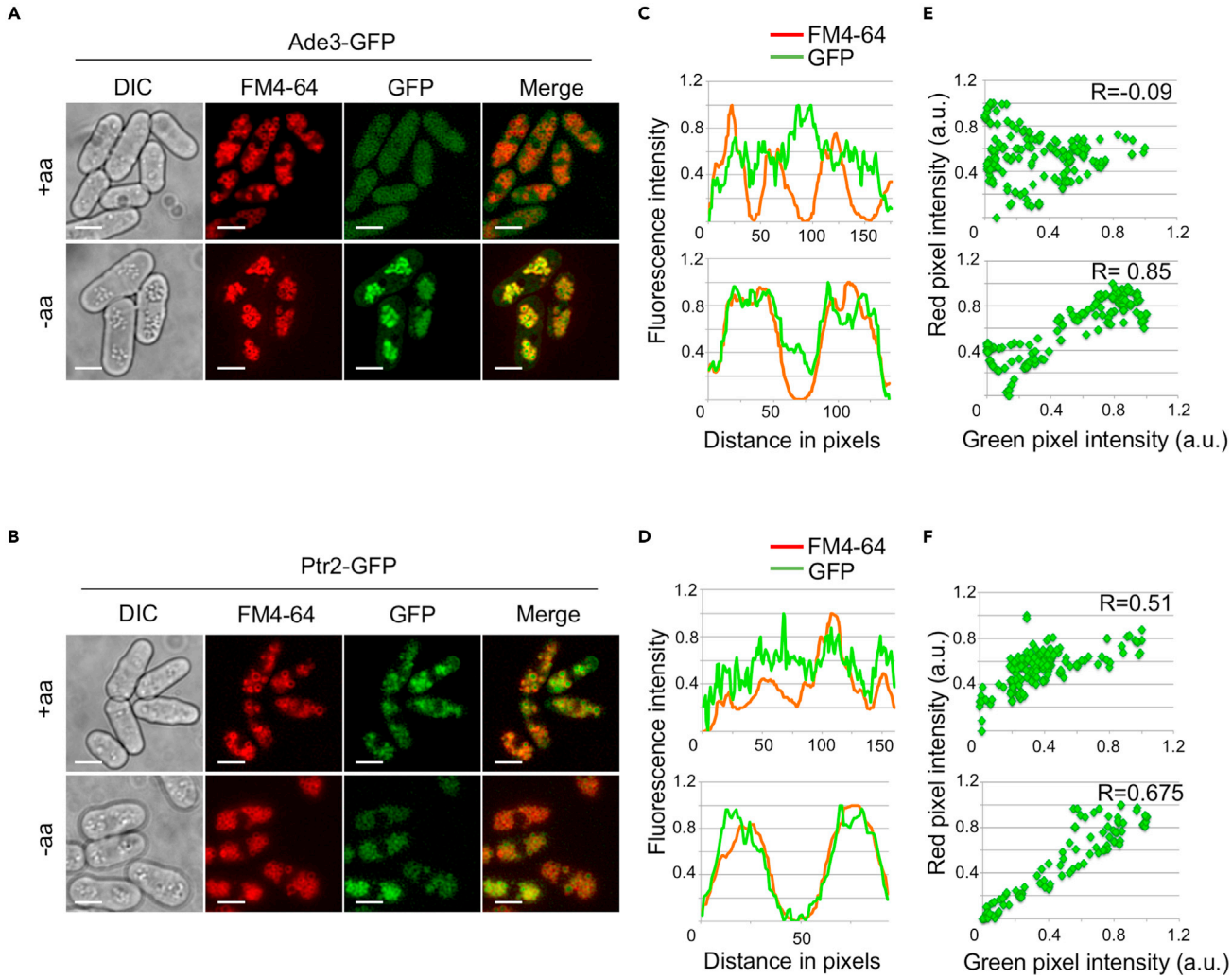

Figure 6. Localization of GFP-tagged Ade3 and Ptr2 in response to amino acid starvation

Representative fluorescence microscopy images depicting the co-localization of (A) Ade3-GFP and (B) Ptr2-GFP with vacuoles (FM4-64-Red) for cells grown continuously in minimal media supplemented with amino acids (+aa) or starved for amino acids for 90 min (-aa). Scale bar – 10μm. Graphs depicting the fluorescence intensity signal of Ade3-GFP (C) and Ptr2-GFP (D) along with FM4-64 after drawing a line from one end of the cell to another. Representative graphs used to calculate the Pearson correlation coefficient (R) of overlap between Ade-GFP (E) and Ptr2-GFP (F) with FM4-64. DIC - differential interference contrast; a.u.– arbitrary units; GFP – green fluorescent protein. 15 cells per replicate were analyzed for calculating R using ImageJ software. Three biological replicates were performed.

See also Figure S7.

such that, depending on the cell type, nutritional or energy status of the cell, FLCN may also act as a TORC1 repressor (Hudon et al., 2010). Future experiments are required to test this hypothesis in mammalian cells.

FLCN interaction with the V-ATPase complex

Previous work in mammalian cells has shown that the vacuolar-type H^+ATPase (V-ATPase) complex plays an important role in amino acid-dependent activation of mTORC1. It acts downstream of the amino acid signal and upstream of Rags, transmitting the amino acid signal from the lysosomal lumen to mTORC1 via Ragulator-Rag complex (Bar-Peled et al., 2012; Zoncu et al., 2011). Here, our data suggest that BFC physically associated with Vma2 and other subunits of the V-ATPase complex, and regulates its activity in an amino acid-dependent manner (Figures 4 and S6). Moreover, we found that this interaction appears to be conserved in *S. cerevisiae*, highlighting its significance in TORC1 regulation (Figure 4). Based on these,

we hypothesize that the suggested interaction between FLCN protein family members and the V-ATPase complex may be important in amino acid-dependent regulation of TORC1 in eukaryotes. Further experimentation is required to determine whether this interaction is reciprocal in the fission and budding yeast and how FLCN homologs regulate V-ATPase activity in an amino acid-dependent manner.

Ptr2 and Ade3 are involved in amino acid -dependent regulation of TORC1

The comparison of our proteomic (Tables S1 and S2) and the published genetic (Ryan et al., 2012) interaction networks (Table S7) of BFC suggested that Ptr2 and Ade3 also may function to regulate TORC1 in an amino acid-dependent manner. Specifically, all Bhd1-TAP, Fnp1-TAP one-step purifications in *S. pombe* (Tables S1 and S2) and Lst7-TAP purification in *S. cerevisiae* (Table S3) coimmunoprecipitated substoichiometric amount of Ptr2 and Ade3 (called Ptr2 and Ade6 in *S. cerevisiae*), suggesting that this interaction may be conserved in these two distantly related yeast species. Also, *ptr2* and *ade3* genes display high similarity scores with the genetic interaction network of *bhd1* and *fnp1* (Table S7) (Ryan et al., 2012). Here, we found that both Ptr2 and Ade3, similar to BFC, are resistant to rapamycin and that these proteins are required for efficient repression of TORC1 in response to amino acid starvation (Figure 5). Furthermore, Ade3-GFP, whose signal is diffuse when cells are grown on media supplemented with amino acids, localizes to vacuoles upon amino acid starvation (Figure 6). Ptr2-GFP, on the other hand, is found primarily at vacuoles under both amino acid replete and starved conditions, and its absence results in the amino acid-independent recruitment of BFC to vacuoles. Ptr2 is a member of a highly conserved dipeptide transport family in eukaryotes which in *S. pombe* has been shown to be required for transport of di- and tripeptides (Kitamura et al., 2017). Its localization to vacuoles under amino acid replete and starved conditions suggests that this protein may function to regulate TORC1 activity in response to amino acid signal by transmitting the intravacuolar amino acid status to TORC1. Interestingly, recent papers have revealed that the mammalian homolog of Ptr2, SLC15A4, is lysosomal and interacts with and critically regulates the activity of mTOR in macrophages (Kobayashi et al., 2014, 2021a, 2021b). These observations suggest that the regulation of TORC1 by Ptr2 family of proteins is an ancient regulatory mechanism which in mammals can be used to couple and regulate the metabolic and immunological activities of immune cells (Toyama-Sorimachi and Kobayashi, 2021).

It was surprising to discover that Ade3, a phosphoribosylformylglycinamidine synthase enzyme whose only known activity is in adenine biosynthesis, is also required for efficient repression of TORC1 when cells are starved for amino acids. Interestingly, we found that previous purification of the mammalian FLCN yielded the co-immunoprecipitation of GART, an Ade1/Ade5 homolog involved in purine synthesis in human cells. Could a protein involved in purine biosynthesis also function in the amino acid-dependent repression of TORC1? But how could the two processes be connected? It is well established that TORC1 activation stimulates ribosome biogenesis to meet the increasing demand for protein synthesis (Iadevaia et al., 2014). TORC1 activation stimulates RNA Pol I and Pol III-mediated transcription of ribosome RNAs (rRNAs), synthesis of ribosomal proteins and other components required for ribosome formation. This depletes the intracellular pools of both amino acids and nucleotides. To meet the increasing need for nucleotides, recent work has shown that TORC1 activation also upregulates purine and pyrimidine biosynthesis (Ben-Sahra et al., 2013, 2016; Robitaille et al., 2013) and that TORC1 signaling network can sense and modulate TORC1 activity in response to intracellular levels of purines (Hoxhaj et al., 2017). Here, (1) the requirement for Ade3 in amino acid-dependent repression of TORC1 (Figure 5), (2) the enrichment of purine biosynthesis as one of the main gene ontology pathways enriched in all Fnp1-and Bhd1-TAP one-step purifications (Tables S1 and S2), (3) the coimmunoprecipitation of several adenine biosynthetic proteins in addition to Ade6, the budding yeast homolog of *S. pombe* Ade3, in our Lst7-TAP purification in *S. cerevisiae* (ADE2, ADE3, ADE5, ADE12) (Table S3), and (4) coimmunoprecipitation of GART, the Ade1/Ade5 homolog in FLCN purification (Table S4) (Laviolette et al., 2017) suggest that purine sensing and biosynthesis pathway may intersect with the amino acid-dependent regulation of TORC1, providing a dual sensing mechanism which converge on TORC1 in *S. pombe*. This, we hypothesize, could couple amino acid and nucleotide biosynthetic and sensing pathways which are essential for increasing the capacity of the cell to synthesize ribosomes and therefore proteins. Further experiments are required to determine whether this regulatory intersection is conserved in other eukaryotes.

Overall, in this paper, by characterizing the Bhd1-Fnp1 complex (BFC) in the fission yeast, we show that BFC not only can act as an activator of TORC1 upon amino acid stimulation but also can augment TORC1 repression when cells are starved for amino acids, suggesting that its activity is akin to a rheostat, tuning TORC1

activity in a context-dependent manner. Future experiments are required to determine whether this activity is conserved in human cells, particularly in RCC where FLCN acts as a tumor suppressor protein. Moreover, the proteomic and genetic interaction networks of BFC in *S. pombe* helped identify several highly conserved proteins which we show are also involved in amino acid dependent regulation of TORC1. Considering the conservation of amino acid-dependent regulation of TORC1 in *S. pombe* relative to the human TORC1 system, our data establish the fission yeast as an excellent model for uncovering the molecular mechanisms by which FLCN and auxiliary proteins repress TORC1 in response to amino acid starvation in eukaryotes.

Limitation of the study

Our data reveal that immunoprecipitation of FLCN-containing complexes in the fission and budding yeasts co-immunoprecipitated Vma2 and other components of the V-ATPase complex. We also found that in the fission yeast BFC regulates the V-ATPase complex activity in an amino acid-dependent manner. Even though these data suggest that the physical interaction between BFC and the V-ATPase complex is required for the amino acid-dependent regulation of the V-ATPase complex, reciprocal co-IPs among BFC and the V-ATPase components are needed to test this hypothesis. Also, all the Western blots in which the level of phosphor-Rps6 was measured, tubulin was used as our loading control. This is because we were unable to find a commercial source for an antibody against the total Rps6 protein in *pombe*.

STAR★METHODS

Detailed methods are provided in the online version of this paper and include the following:

- KEY RESOURCES TABLE
- RESOURCE AVAILABILITY
  - Lead contact
  - Materials availability
  - Data and code availability
- EXPERIMENTAL MODEL AND SUBJECT DETAILS
  - Strain construction
  - Yeast growth assays, amino acid starvation and amino acid supplementation
- METHOD DETAILS
  - Tandem affinity purification
  - Liquid chromatography and tandem mass spectrometry
  - Proteomic data analysis
  - Structure-based sequence alignments
  - Protein co-immunoprecipitation assays
  - Fluorescence microscopy of GFP-tagged proteins
  - Vacuolar pH determination
  - Trichloroacetic acid (TCA) protein extracts and immunoblot analysis
  - *S. cerevisiae* growth C = conditions and protein co-immunoprecipitation assay
  - Rapamycin, bafilomycin and alkaline pH plate sensitivity assays by serial dilution
- QUANTIFICATION AND STATISTICAL ANALYSIS

SUPPLEMENTAL INFORMATION

Supplemental information can be found online at https://doi.org/10.1016/j.isci.2021.103338.

ACKNOWLEDGMENTS

MM was supported by a V Scholar, ACS Research Scholar grant (18-056-01-RMC) and R01 (GM125782). IAC was supported by a Beatriu de Pinos (Generalitat de Catalunya) postdoctoral fellowship. JAP is supported by NIHgrant (GM132129). SPG is supported by NIHgrant (GM67945), and OI is supported by a DODgrant (W81XWH-19-1-0855). A.B. was supported by a Schrödinger Fellowship (J3872-B21) from the Austrian Science Fund and a fellowship from theAmerican Heart Association (19POST34380800). Dr. Stephen Buratowski generously provided us with the BY4741 and *LST7-TAP S. cerevisiae* strains. We thank Andria Augur and Ben Wardwell for technical assistance and the members of the Motamedi Lab for critical reading and constructive comments on the manuscript. We are especially thankful to Dr. Linda Niemann for technical help with microscopy image processing and analyses.

AUTHOR CONTRIBUTIONS

MM and OI conceived the research project. MM directed the study. IAC, SS and AODG conducted the studies and wrote the paper. SPG and JAP performed the mass spectrometry experiments and JZ helped in proteomic data analysis. HA and AB performed the homology and structural modeling analysis for Fnp1. AODG constructed several strains and performed steady-state growth and nitrogen source experiments. JML helped in strain construction, microscopy and starvation/TORC1 activity experiments. CMP and LAL performed one of the Bhd1/Lst7 purifications.

DECLARATION OF INTERESTS

The authors declare no competing interests.

Received: March 9, 2021
Revised: June 10, 2021
Accepted: October 21, 2021
Published: November 19, 2021

REFERENCES

Alfa, C. (1993). Experiments with Fission Yeast: A Laboratory Course Manual (Cold Spring Harbor Laboratory Press).

Alvarez, B., and Moreno, S. (2006). Fission yeast Tor2 promotes cell growth and represses cell differentiation. J. Cell Sci. *119*, 4475–4485.

Baba, M., Furihata, M., Hong, S.B., Tessarollo, L., Haines, D.C., Southon, E., Patel, V., Igarashi, P., Alvord, W.G., Leighty, R., et al. (2008). Kidney-targeted Birt-Hogg-Dube gene inactivation in a mouse model: Erk1/2 and Akt-mTOR activation, cell hyperproliferation, and polycystic kidneys. J. Natl. Cancer Inst. *100*, 140–154.

Baba, M., Hong, S.B., Sharma, N., Warren, M.B., Nickerson, M.L., Iwamatsu, A., Esposito, D., Gillette, W.K., Hopkins, R.F., 3rd, Hartley, J.L., et al. (2006). Folliculin encoded by the BHD gene interacts with a binding protein, FNIP1, and AMPK, and is involved in AMPK and mTOR signaling. Proc. Natl. Acad. Sci. U S A *103*, 15552–15557.

Bahler, J., Wu, J.Q., Longtine, M.S., Shah, N.G., McKenzie, A., 3rd, Steever, A.B., Wach, A., Philippsen, P., and Pringle, J.R. (1998). Heterologous modules for efficient and versatile PCR-based gene targeting in Schizosaccharomyces pombe. Yeast *14*, 943–951.

Bar-Peled, L., Chantranupong, L., Cherniack, A.D., Chen, W.W., Ottina, K.A., Grabiner, B.C., Spear, E.D., Carter, S.L., Meyerson, M., and Sabatini, D.M. (2013). A Tumor suppressor complex with GAP activity for the Rag GTPases that signal amino acid sufficiency to mTORC1. Science *340*, 1100–1106.

Bar-Peled, L., and Sabatini, D.M. (2014). Regulation of mTORC1 by amino acids. Trends Cell Biol. *24*, 400–406.

Bar-Peled, L., Schweitzer, L.D., Zoncu, R., and Sabatini, D.M. (2012). Ragulator is a GEF for the rag GTPases that signal amino acid levels to mTORC1. Cell *150*, 1196–1208.

Beausoleil, S.A., Villen, J., Gerber, S.A., Rush, J., and Gygi, S.P. (2006). A probability-based approach for high-throughput protein phosphorylation analysis and site localization. Nat. Biotechnol. *24*, 1285–1292.

Ben-Sahra, I., Howell, J.J., Asara, J.M., and Manning, B.D. (2013). Stimulation of de novo pyrimidine synthesis by growth signaling through mTOR and S6K1. Science *339*, 1323–1328.

Ben-Sahra, I., Hoxhaj, G., Ricoult, S.J.H., Asara, J.M., and Manning, B.D. (2016). mTORC1 induces purine synthesis through control of the mitochondrial tetrahydrofolate cycle. Science *351*, 728–733.

Binda, M., Peli-Gulli, M.P., Bonfils, G., Panchaud, N., Urban, J., Sturgill, T.W., Loewith, R., and De Virgilio, C. (2009). The Vam6 GEF controls TORC1 by activating the EGO complex. Mol. Cell *35*, 563–573.

Birt, A.R., Hogg, G.R., and Dube, W.J. (1977). Hereditary multiple fibrofolliculomas with trichodiscomas and acrochordons. Arch. Dermatol. *113*, 1674–1677.

Brazer, S.C., Williams, H.P., Chappell, T.G., and Cande, W.Z. (2000). A fission yeast kinesin affects Golgi membrane recycling. Yeast *16*, 149–166.

Bruar, M., et al. (2008). Coordination of growth rate, cell cycle, stress response, and metabolic activity in yeast. Mol Biol Cell *19*, 352–367.

Chen, J., Futami, K., Petillo, D., Peng, J., Wang, P., Knol, J., Li, Y., Khoo, S.K., Huang, D., Qian, C.N., et al. (2008). Deficiency of FLCN in mouse kidney led to development of polycystic kidneys and renal neoplasia. PLoS One *3*, e3581.

Chia, K.H., Fukuda, T., Sofyantoro, F., Matsuda, T., Amai, T., and Shiozaki, K. (2017). Ragulator and GATOR1 complexes promote fission yeast growth by attenuating TOR complex 1 through Rag GTPases. Elife *6*, e30880.

Chica, N., Rozalen, A.E., Perez-Hidalgo, L., Rubio, A., Novak, B., and Moreno, S. (2016). Nutritional control of cell size by the Greatwall-Endosulfine-PP2A.B55 pathway. Curr. Biol. *26*, 319–330.

Cummings, M.T., Joh, R.I., and Motamedi, M. (2015). PRIMED: PRIMEr database for deleting and tagging all fission and budding yeast genes developed using the open-source genome retrieval script (GRS). PLoS One *10*, e0116657.

Elias, J.E., and Gygi, S.P. (2007). Target-decoy search strategy for increased confidence in large-scale protein identifications by mass spectrometry. Nat. Methods *4*, 207–214.

Elias, J.E., and Gygi, S.P. (2010). Target-decoy search strategy for mass spectrometry-based proteomics. Methods Mol. Biol. *604*, 55–71.

Eng, J.K., Jahan, T.A., and Hoopmann, M.R. (2013). Comet: an open-source MS/MS sequence database search tool. Proteomics *13*, 22–24.

Engel, R. (2004). The Molecular Biology of Schizosaccharomyces Pombe (Springer).

Fukuda, T., Sofyantoro, F., Tai, Y.T., Chia, K.H., Matsuda, T., Murase, T., Morozumi, Y., Tatebe, H., Kanki, T., and Shiozaki, K. (2021). Tripartite suppression of fission yeast TORC1 signaling by the GATOR1-Sea3 complex, the TSC complex, and Gcn2 kinase. Elife *10*, e60969.

Gonzalez, A., Hall, M.N., Lin, S.C., and Hardie, D.G. (2020). AMPK and TOR: the yin and yang of cellular nutrient sensing and growth control. Cell Metab. *31*, 472–492.

Hara, K., Yonezawa, K., Weng, Q.P., Kozlowski, M.T., Belham, C., and Avruch, J. (1998). Amino acid sufficiency and mTOR regulate p70 S6 kinase and eIF-4E BP1 through a common effector mechanism. J. Biol. Chem. *273*, 14484–14494.

Hasumi, H., Baba, M., Hong, S.B., Hasumi, Y., Huang, Y., Yao, M., Valera, V.A., Linehan, W.M., and Schmidt, L.S. (2008). Identification and characterization of a novel folliculin-interacting protein FNIP2. Gene *415*, 60–67.

Hasumi, Y., Baba, M., Ajima, R., Hasumi, H., Valera, V.A., Klein, M.E., Haines, D.C., Merino, M.J., Hong, S.B., Yamaguchi, T.P., et al. (2009). Homozygous loss of BHD causes early embryonic lethality and kidney tumor development with activation of mTORC1 and mTORC2. Proc. Natl. Acad. Sci. U S A *106*, 18722–18727.

Hayashi, T., Hatanaka, M., Nagao, K., Nakaseko, Y., Kanoh, J., Kokubu, A., Ebe, M., and Yanagida,

M. (2007). Rapamycin sensitivity of the Schizosaccharomyces pombe tor2 mutant and organization of two highly phosphorylated TOR complexes by specific and common subunits. Genes Cells *12*, 1357–1370.

Hentges, P., Van Driessche, B., Tafforeau, L., Vandenhaute, J., and Carr, A.M. (2005). Three novel antibiotic marker cassettes for gene disruption and marker switching in Schizosaccharomyces pombe. Yeast *22*, 1013–1019.

Hirose, E., Nakashima, N., Sekiguchi, T., and Nishimoto, T. (1998). Raga is a functional homologue of S. cerevisiae Gtr1p involved in the Ran/Gsp1-GTPase pathway. J. Cell Sci. *111* (Pt 1), 11–21.

Hoxhaj, G., Hughes-Hallett, J., Timson, R.C., Ilagan, E., Yuan, M., Asara, J.M., Ben-Sahra, I., and Manning, B.D. (2017). The mTORC1 signaling network senses changes in cellular purine nucleotide levels. Cell Rep. *21*, 1331–1346.

Hua, H., Kong, Q., Zhang, H., Wang, J., Luo, T., and Jiang, Y. (2019). Targeting mTOR for cancer therapy. J. Hematol.Oncol. *12*, 71.

Hudon, V., Sabourin, S., Dydensborg, A.B., Kottis, V., Ghazi, A., Paquet, M., Crosby, K., Pomerleau, V., Uetani, N., and Pause, A. (2010). Renal tumour suppressor function of the Birt-Hogg-Dube syndrome gene product folliculin. J. Med. Genet. *47*, 182–189.

Huttlin, E.L., Jedrychowski, M.P., Elias, J.E., Goswami, T., Rad, R., Beausoleil, S.A., Villen, J., Haas, W., Sowa, M.E., and Gygi, S.P. (2010). A tissue-specific atlas of mouse protein phosphorylation and expression. Cell *143*, 1174–1189.

Iadevaia, V., Liu, R., and Proud, C.G. (2014). mTORC1 signaling controls multiple steps in ribosome biogenesis. Semin. Cell Dev. Biol. *36*, 113–120.

Iwaki, T., Goa, T., Tanaka, N., and Takegawa, K. (2004). Characterization of Schizosaccharomyces pombe mutants defective in vacuolar acidification and protein sorting. Mol. Genet. Genomics *271*, 197–207.

Iwaki, T., Osawa, F., Onishi, M., Koga, T., Fujita, Y., Hosomi, A., Tanaka, N., Fukui, Y., and Takegawa, K. (2003). Characterization of vps33+, a gene required for vacuolar biogenesis and protein sorting in Schizosaccharomyces pombe. Yeast *20*, 845–855.

Jewell, J.L., Russell, R.C., and Guan, K.L. (2013). Amino acid signalling upstream of mTOR. Nat. Rev. Mol. Cell Biol. *14*, 133–139.

Joh, R.I., Khanduja, J.S., Calvo, I.A., Mistry, M., Palmieri, C.M., Savol, A.J., Ho Sui, S.J., Sadreyev, R.I., Aryee, M.J., and Motamedi, M. (2016). Survival in quiescence requires the euchromatic deployment of Clr4/SUV39H by Argonaute-associated small RNAs. Mol. Cell *64*, 1088–1101.

Jung, J., Genau, H.M., and Behrends, C. (2015). Amino acid-dependent mTORC1 regulation by the lysosomal membrane protein SLC38A9. Mol. Cell Biol. *35*, 2479–2494.

Kashiwazaki, J., Iwaki, T., Takegawa, K., Shimoda, C., and Nakamura, T. (2009). Two fission yeast rab7 homologs, ypt7 and ypt71, play antagonistic roles in the regulation of vacuolar morphology. Traffic *10*, 912–924.

Kato, T., Pothula, S., Liu, R.J., Duman, C.H., Terwilliger, R., Vlasuk, G.P., Saiah, E., Hahm, S., and Duman, R.S. (2019). Sestrin modulator NV-5138 produces rapid antidepressant effects via direct mTORC1 activation. J. Clin. Invest. *129*, 2542–2554.

Kelley, L.A., Mezulis, S., Yates, C.M., Wass, M.N., and Sternberg, M.J. (2015). The Phyre2 web portal for protein modeling, prediction and analysis. Nat. Protoc. *10*, 845–858.

Khoo, S.K., Bradley, M., Wong, F.K., Hedblad, M.A., Nordenskjold, M., and Teh, B.T. (2001). Birt-Hogg-Dube syndrome: mapping of a novel hereditary neoplasia gene to chromosome 17p12-q11.2. Oncogene *20*, 5239–5242.

Khoo, S.K., Kahnoski, K., Sugimura, J., Petillo, D., Chen, J., Shockley, K., Ludlow, J., Knapp, R., Giraud, S., Richard, S., et al. (2003). Inactivation of BHD in sporadic renal tumors. Cancer Res. *63*, 4583–4587.

Kim, E., Goraksha-Hicks, P., Li, L., Neufeld, T.P., and Guan, K.L. (2008). Regulation of TORC1 by Rag GTPases in nutrient response. Nat. Cell Biol. *10*, 935–945.

Kitamura, K., Kinsui, E.Z., and Abe, F. (2017). Critical role of the proton-dependent oligopeptide transporter (POT) in the cellular uptake of the peptidyl nucleoside antibiotic, blasticidin S. Biochim.Biophys. Acta Mol. Cell Res. *1864*, 393–398.

Kobayashi, T., Nguyen-Tien, D., Ohshima, D., Karyu, H., Shimabukuro-Demoto, S., Yoshida-Sugitani, R., and Toyama-Sorimachi, N. (2021a). Human SLC15A4 is crucial for TLR-mediated type I interferon production and mitochondrial integrity. Int. Immunol. *33*, 399–406.

Kobayashi, T., Nguyen-Tien, D., Sorimachi, Y., Sugiura, Y., Suzuki, T., Karyu, H., Shimabukuro-Demoto, S., Uemura, T., Okamura, T., Taguchi, T., et al. (2021b). SLC15A4 mediates M1-prone metabolic shifts in macrophages and guards immune cells from metabolic stress. Proc. Natl. Acad. Sci. U S A *118*, e2100295118.

Kobayashi, T., Shimabukuro-Demoto, S., Yoshida-Sugitani, R., Furuyama-Tanaka, K., Karyu, H., Sugiura, Y., Shimizu, Y., Hosaka, T., Goto, M., Kato, N., et al. (2014). The histidine transporter SLC15A4 coordinates mTOR-dependent inflammatory responses and pathogenic antibody production. Immunity *41*, 375–388.

Laviolette, L.A., Mermoud, J., Calvo, I.A., Olson, N., Boukhali, M., Steinlein, O.K., Roider, E., Sattler, E.C., Huang, D., Teh, B.T., et al. (2017). Negative regulation of EGFR signalling by the human folliculin tumour suppressor protein. Nat. Commun. *8*, 15866.

Li, Y. (2011). The tandem affinity purification technology: an overview. Biotechnol.Lett. *33*, 1487–1499.

Liu, G.Y., and Sabatini, D.M. (2020). mTOR at the nexus of nutrition, growth, ageing and disease. Nat. Rev. Mol. Cell Biol. *21*, 183–203.

Ma, N., Liu, Q., Zhang, L., Henske, E.P., and Ma, Y. (2013). TORC1 signaling is governed by two negative regulators in fission yeast. Genetics *195*, 457–468.

Mach, K.E., Furge, K.A., and Albright, C.F. (2000). Loss of Rhb1, a Rheb-related GTPase in fission yeast, causes growth arrest with a terminal phenotype similar to that caused by nitrogen starvation. Genetics *155*, 611–622.

Marguerat, S., Schmidt, A., Codlin, S., Chen, W., Aebersold, R., and Bahler, J. (2012). Quantitative analysis of fission yeast transcriptomes and proteomes in proliferating and quiescent cells. Cell *151*, 671–683.

Martin, R., Portantier, M., Chica, N., Nyquist-Andersen, M., Mata, J., and Lopez-Aviles, S. (2017). A PP2A-B55-mediated Crosstalk between TORC1 and TORC2 regulates the differentiation response in fission yeast. Curr. Biol. *27*, 175–188.

Matsuda, S., Kikkawa, U., Uda, H., and Nakashima, A. (2020). The S. pombe CDK5 ortholog Pef1 regulates sexual differentiation through control of the TORC1 pathway and autophagy. J. Cell Sci. *133*, jcs247817.

Matsuo, T., Otsubo, Y., Urano, J., Tamanoi, F., and Yamamoto, M. (2007). Loss of the TOR kinase Tor2 mimics nitrogen starvation and activates the sexual development pathway in fission yeast. Mol. Cell Biol. *27*, 3154–3164.

Meng, J., and Ferguson, S.M. (2018). GATOR1-dependent recruitment of FLCN-FNIP to lysosomes coordinates Rag GTPase heterodimer nucleotide status in response to amino acids. J. Cell Biol. *217*, 2765–2776.

Merhi, A., Delree, P., and Marini, A.M. (2017). The metabolic waste ammonium regulates mTORC2 and mTORC1 signaling. Sci. Rep. *7*, 44602.

Motamedi, M.R., Hong, E.J., Li, X., Gerber, S., Denison, C., Gygi, S., and Moazed, D. (2008). HP1 proteins form distinct complexes and mediate heterochromatic gene silencing by nonoverlapping mechanisms. Mol. Cell *32*, 778–790.

Motamedi, M.R., Verdel, A., Colmenares, S.U., Gerber, S.A., Gygi, S.P., and Moazed, D. (2004). Two RNAi complexes, RITS and RDRC, physically interact and localize to noncoding centromeric RNAs. Cell *119*, 789–802.

Nada, S., Hondo, A., Kasai, A., Koike, M., Saito, K., Uchiyama, Y., and Okada, M. (2009). The novel lipid raft adaptor p18 controls endosome dynamics by anchoring the MEK-ERK pathway to late endosomes. EMBO J. *28*, 477–489.

Nakashima, A., Sato, T., and Tamanoi, F. (2010). Fission yeast TORC1 regulates phosphorylation of ribosomal S6 proteins in response to nutrients and its activity is inhibited by rapamycin. J. Cell Sci. *123*, 777–786.

Nakashima, A., and Tamanoi, F. (2010). Conservation of the Tsc/Rheb/TORC1/S6K/S6 signaling in fission yeast. Enzymes *28*, 167–187.

Nakashima, N., Noguchi, E., and Nishimoto, T. (1999). Saccharomyces cerevisiae putative G protein, Gtr1p, which forms complexes with itself and a novel protein designated as Gtr2p,

negatively regulates the Ran/Gsp1p G protein cycle through Gtr2p. Genetics *152*, 853–867.

Nickerson, M.L., Warren, M.B., Toro, J.R., Matrosova, V., Glenn, G., Turner, M.L., Duray, P., Merino, M., Choyke, P., Pavlovich, C.P., et al. (2002). Mutations in a novel gene lead to kidney tumors, lung wall defects, and benign tumors of the hair follicle in patients with the Birt-Hogg-Dube syndrome. Cancer Cell *2*, 157–164.

Nookala, R.K., Langemeyer, L., Pacitto, A., Ochoa-Montano, B., Donaldson, J.C., Blaszczyk, B.K., Chirgadze, D.Y., Barr, F.A., Bazan, J.F., and Blundell, T.L. (2012). Crystal structure of folliculin reveals a hidDENN function in genetically inherited renal cancer. Open Biol. *2*, 120071.

Pacitto, A., Ascher, D.B., Wong, L.H., Blaszczyk, B.K., Nookala, R.K., Zhang, N., Dokudovskaya, S., Levine, T.P., and Blundell, T.L. (2015). Lst4, the yeast Fnip1/2 orthologue, is a DENN-family protein. Open Biol. *5*, 150174.

Paulo, J.A. (2016). Sample preparation for proteomic analysis using a GeLC-MS/MS strategy. J. Biol. Methods *3*, e45.

Péli-Gulli, M.-P., Sardu, A., Panchaud, N., Raucci, S., and De Virgilio, C. (2015). Amino acids stimulate TORC1 through lst4-lst7, a GTPase-activating protein complex for the rag family GTPase Gtr2. Cell Rep. *13*, 1–7.

Peli-Gulli, M.P., Raucci, S., Hu, Z., Dengjel, J., and De Virgilio, C. (2017). Feedback inhibition of the rag GTPase GAP complex lst4-lst7 Safeguards TORC1 from hyperactivation by amino acid signals. Cell Rep. *20*, 281–288.

Perzov, N., Padler-Karavani, V., Nelson, H., and Nelson, N. (2002). Characterization of yeast V-ATPase mutants lacking Vph1p or Stv1p and the effect on endocytosis. J. Exp. Biol. *205*, 1209–1219.

Petit, C.S., Roczniak-Ferguson, A., and Ferguson, S.M. (2013). Recruitment of folliculin to lysosomes supports the amino acid-dependent activation of Rag GTPases. J. Cell Biol. *202*, 1107–1122.

Price, A., Seals, D., Wickner, W., and Ungermann, C. (2000). The docking stage of yeast vacuole fusion requires the transfer of proteins from a cis-SNARE complex to a Rab/Ypt protein. J. Cell Biol. *148*, 1231–1238.

Rebsamen, M., Pochini, L., Stasyk, T., de Araujo, M.E., Galluccio, M., Kandasamy, R.K., Snijder, B., Fauster, A., Rudashevskaya, E.L., Bruckner, M., et al. (2015). SLC38A9 is a component of the lysosomal amino acid sensing machinery that controls mTORC1. Nature *519*, 477–481.

Rigaut, G., Shevchenko, A., Rutz, B., Wilm, M., Mann, M., and Seraphin, B. (1999). A generic protein purification method for protein complex characterization and proteome exploration. Nat. Biotechnol. *17*, 1030–1032.

Robitaille, A.M., Christen, S., Shimobayashi, M., Cornu, M., Fava, L.L., Moes, S., Prescianotto-Baschong, C., Sauer, U., Jenoe, P., and Hall, M.N. (2013). Quantitative phosphoproteomics reveal mTORC1 activates de novo pyrimidine synthesis. Science *339*, 1320–1323.

Rodland, G.E., Tvegard, T., Boye, E., and Grallert, B. (2014). Crosstalk between the Tor and Gcn2 pathways in response to different stresses. Cell Cycle *13*, 453–461.

Rogala, K.B., Gu, X., Kedir, J.F., Abu-Remaileh, M., Bianchi, L.F., Bottino, A.M.S., Dueholm, R., Niehaus, A., Overwijn, D., Fils, A.P., et al. (2019). Structural basis for the docking of mTORC1 on the lysosomal surface. Science *366*, 468–475.

Ryan, C.J., Roguev, A., Patrick, K., Xu, J., Jahari, H., Tong, Z., Beltrao, P., Shales, M., Qu, H., Collins, S.R., et al. (2012). Hierarchical modularity and the evolution of genetic interactomes across species. Mol. Cell *46*, 691–704.

Sancak, Y., Bar-Peled, L., Zoncu, R., Markhard, A.L., Nada, S., and Sabatini, D.M. (2010). Ragulator-Rag complex targets mTORC1 to the lysosomal surface and is necessary for its activation by amino acids. Cell *141*, 290–303.

Sancak, Y., Peterson, T.R., Shaul, Y.D., Lindquist, R.A., Thoreen, C.C., Bar-Peled, L., and Sabatini, D.M. (2008). The Rag GTPases bind raptor and mediate amino acid signaling to mTORC1. Science *320*, 1496–1501.

Sato, M., Dhut, S., and Toda, T. (2005). New drug-resistant cassettes for gene disruption and epitope tagging in Schizosaccharomyces pombe. Yeast *22*, 583–591.

Saxton, R.A., and Sabatini, D.M. (2017). mTOR signaling in growth, metabolism, and disease. Cell *169*, 361–371.

Schmidt, L.S., Warren, M.B., Nickerson, M.L., Weirich, G., Matrosova, V., Toro, J.R., Turner, M.L., Duray, P., Merino, M., Hewitt, S., et al. (2001). Birt-Hogg-Dube syndrome, a genodermatosis associated with spontaneous pneumothorax and kidney neoplasia, maps to chromosome 17p11.2. Am. J. Hum.Genet. *69*, 876–882.

Schurmann, A., Brauers, A., Massmann, S., Becker, W., and Joost, H.G. (1995). Cloning of a novel family of mammalian GTP-binding proteins (Raga, RagBs, RagB1) with remote similarity to the Ras-related GTPases. J. Biol. Chem. *270*, 28982–28988.

Sekiguchi, T., Hirose, E., Nakashima, N., Ii, M., and Nishimoto, T. (2001). Novel G proteins, rag C and rag D, interact with GTP-binding proteins, rag A and rag B. J. Biol. Chem. *276*, 7246–7257.

Sengupta, S., Giaime, E., Narayan, S., Hahm, S., Howell, J., O'Neill, D., Vlasuk, G.P., and Saiah, E. (2019). Discovery of NV-5138, the first selective Brain mTORC1 activator. Sci. Rep. *9*, 4107.

Shen, K., Rogala, K.B., Chou, H.T., Huang, R.K., Yu, Z., and Sabatini, D.M. (2019). Cryo-EM structure of the human FLCN-FNIP2-rag-Ragulator complex. Cell *179*, 1319–1329.e8.

Shimanuki, M., Chung, S.Y., Chikashige, Y., Kawasaki, Y., Uehara, L., Tsutsumi, C., Hatanaka, M., Hiraoka, Y., Nagao, K., and Yanagida, M. (2007). Two-step, extensive alterations in the transcriptome from G0 arrest to cell division in Schizosaccharomyces pombe. Genes Cells *12*, 677–692.

Takagi, Y., Kobayashi, T., Shiono, M., Wang, L., Piao, X., Sun, G., Zhang, D., Abe, M., Hagiwara, Y., Takahashi, K., et al. (2008). Interaction of folliculin (Birt-Hogg-Dube gene product) with a novel Fnip1-like (FnipL/Fnip2) protein. Oncogene *27*, 5339–5347.

Tatebe, H., and Shiozaki, K. (2017). Evolutionary conservation of the components in the TOR signaling pathways. Biomolecules *7*, 77.

Toro, J.R., Glenn, G., Duray, P., Darling, T., Weirich, G., Zbar, B., Linehan, M., and Turner, M.L. (1999). Birt-Hogg-Dube syndrome: a novel marker of kidney neoplasia. Arch. Dermatol. *135*, 1195–1202.

Toyama-Sorimachi, N., and Kobayashi, T. (2021). Lysosomal amino acid transporters as key players in inflammatory diseases. Int. Immunol. dxab069.

Tsun, Z.Y., Bar-Peled, L., Chantranupong, L., Zoncu, R., Wang, T., Kim, C., Spooner, E., and Sabatini, D.M. (2013). The folliculin tumor suppressor is a GAP for the RagC/D GTPases that signal amino acid levels to mTORC1. Mol. Cell *52*, 495–505.

Urano, J., Comiso, M.J., Guo, L., Aspuria, P.J., Deniskin, R., Tabancay, A.P., Jr., Kato-Stankiewicz, J., and Tamanoi, F. (2005). Identification of novel single amino acid changes that result in hyperactivation of the unique GTPase, Rheb, in fission yeast. Mol. Microbiol. *58*, 1074–1086.

Urano, J., Tabancay, A.P., Yang, W., and Tamanoi, F. (2000). The Saccharomyces cerevisiae Rheb G-protein is involved in regulating canavanine resistance and arginine uptake. J. Biol. Chem. *275*, 11198–11206.

Uritani, M., Hidaka, H., Hotta, Y., Ueno, M., Ushimaru, T., and Toda, T. (2006). Fission yeast Tor2 links nitrogen signals to cell proliferation and acts downstream of the Rheb GTPase. Genes Cells *11*, 1367–1379.

Valbuena, N., Guan, K.L., and Moreno, S. (2012a). The Vam6 and Gtr1-Gtr2 pathway activates TORC1 in response to amino acids in fission yeast. J. Cell Sci. *125*, 1920–1928.

Valbuena, N., Rozalen, A.E., and Moreno, S. (2012b). Fission yeast TORC1 prevents eIF2alpha phosphorylation in response to nitrogen and amino acids via Gcn2 kinase. J. Cell Sci. *125*, 5955–5959.

Valvezan, A.J., and Manning, B.D. (2019). Molecular logic of mTORC1 signalling as a metabolic rheostat. Nat. Metab. *1*, 321–333.

van Slegtenhorst, M., Khabibullin, D., Hartman, T.R., Nicolas, E., Kruger, W.D., and Henske, E.P. (2007). The Birt-Hogg-Dube and tuberous sclerosis complex homologs have opposing roles in amino acid homeostasis in Schizosaccharomyces pombe. J. Biol. Chem. *282*, 24583–24590.

Vida, T.A., and Emr, S.D. (1995). A new vital stain for visualizing vacuolar membrane dynamics and endocytosis in yeast. J. Cell Biol. *128*, 779–792.

Vocke, C.D., Yang, Y., Pavlovich, C.P., Schmidt, L.S., Nickerson, M.L., Torres-Cabala, C.A., Merino, M.J., Walther, M.M., Zbar, B., and Linehan, W.M. (2005). High frequency of somatic frameshift BHD gene mutations in

Birt-Hogg-Dube-associated renal tumors. J. Natl. Cancer Inst. *97*, 931–935.

Wang, S., Tsun, Z.Y., Wolfson, R.L., Shen, K., Wyant, G.A., Plovanich, M.E., Yuan, E.D., Jones, T.D., Chantranupong, L., Comb, W., et al. (2015). Metabolism. Lysosomal amino acid transporter SLC38A9 signals arginine sufficiency to mTORC1. Science *347*, 188–194.

Wang, X., Campbell, L.E., Miller, C.M., and Proud, C.G. (1998). Amino acid availability regulates p70 S6 kinase and multiple translation factors. Biochem. J. *334* (Pt 1), 261–267.

Warren, M.B., Torres-Cabala, C.A., Turner, M.L., Merino, M.J., Matrosova, V.Y., Nickerson, M.L., Ma, W., Linehan, W.M., Zbar, B., and Schmidt, L.S. (2004). Expression of Birt-Hogg-Dube gene mRNA in normal and neoplastic human tissues. Mod.Pathol. *17*, 998–1011.

Wiame, J.M., Grenson, M., and Arst, H.N., Jr. (1985). Nitrogen catabolite repression in yeasts and filamentous fungi. Adv. Microb. Physiol. *26*, 1–88.

Wolfson, R.L., and Sabatini, D.M. (2017). The Dawn of the age of amino acid sensors for the mTORC1 pathway. Cell Metab. *26*, 301–309.

Wu, M., Si, S., Li, Y., Schoen, S., Xiao, G.Q., Li, X., Teh, B.T., Wu, G., and Chen, J. (2015). Flcn-deficient renal cells are tumorigenic and sensitive to mTOR suppression. Oncotarget *6*, 32761–32773.

Wunderlich, W., Fialka, I., Teis, D., Alpi, A., Pfeifer, A., Parton, R.G., Lottspeich, F., and Huber, L.A. (2001). A novel 14-kilodalton protein interacts with the mitogen-activated protein kinase scaffold mp1 on a late endosomal/lysosomal compartment. J. Cell Biol. *152*, 765–776.

Wurmser, A.E., Sato, T.K., and Emr, S.D. (2000). New component of the vacuolar class C-Vps complex couples nucleotide exchange on the Ypt7 GTPase to SNARE-dependent docking and fusion. J. Cell Biol. *151*, 551–562.

Zbar, B., Alvord, W.G., Glenn, G., Turner, M., Pavlovich, C.P., Schmidt, L., Walther, M., Choyke, P., Weirich, G., Hewitt, S.M., et al. (2002). Risk of renal and colonic neoplasms and spontaneous pneumothorax in the Birt-Hogg-Dube syndrome. Cancer Epidemiol. Biomarkers Prev. *11*, 393–400.

Zoncu, R., Bar-Peled, L., Efeyan, A., Wang, S., Sancak, Y., and Sabatini, D.M. (2011). mTORC1 senses lysosomal amino acids through an inside-out mechanism that requires the vacuolar H(+)-ATPase. Science *334*, 678–683.

STAR★METHODS

KEY RESOURCES TABLE

REAGENT or RESOURCE	SOURCE	IDENTIFIER
Antibodies		
Affinity-purified Rabbit3 peroxidase anti-peroxidase soluble complex	Sigma-Aldrich	Cat#P1291; RRID: AB_1079562
Mouse monoclonal, anti-c-myc (clone 9 × 10^{11})	Covance Inc.	Cat#MMS-150P; RRID:AB_291323
Mouse monoclonal, anti-FLAG M2-peroxidase antibody (clone M2)	Sigma-Aldrich	Cat#A8592; RRID:AB_439702
Mouse monoclonal, anti-GFP (clone GFP-20)	Sigma-Aldrich	Cat#G6539; RRID:AB_259941
Mouse monoclonal, anti-α-tubulin (clone B-5-1-2)	Sigma-Aldrich	Cat#T6074; RRID:AB_477582
Rabbit monoclonal, anti-phospho-S6 ribosomal protein (Ser235/236) (clone D57.2.2E)	Cell Signaling Technology	Cat#4858; RRID:AB_916156
Mouse monoclonal, anti-actin, pan Ab-5, (clone ACTN05)	Thermo Fisher Scientific	Cat#MS1295P; RRID:AB_63316
Mouse monoclonal, anti-c-myc direct-blot HRP (clone 9E10)	BioLegend	Cat#626803; RRID:AB_626803
HRP-conjugated anti-rabbit IgG	GE healthcare	Cat#NA934; RRID:AB_772206
HRP-conjugated anti-mouse IgG	GE healthcare	Cat#NA931; RRID:AB_772210
Mouse monoclonal anti-Vma2 (clone 13D11B2)	Abcam	Cat#ab113684; RRID:AB_10858975
Chemicals, peptides, and recombinant proteins		
FM4–64 dye	Thermo Fisher Scientific	Cat#T3166
Rapamycin	LC Laboratories	Cat#R5000
Lysosensor green DND-189	Thermo Fisher Scientific	Cat#L7535
Bafilomycin B1 from *Streptomyces sp.*	Sigma-Aldrich	Cat#11707
IgG sepharose 6 fast flow	Cytiva	Cat#17-0969-01
Anti-FLAG M2 affinity gel	Millipore-Sigma	Cat#F2426
Silver nitrate	Fisher chemicals	Cat#S-181-25
Simply blue safe stain	Thermo Fisher Scientific	Cat#LC6065
Trichloroacetic acid	Sigma-Aldrich	Cat#T6399
SuperSignal™west pico PLUS chemiluminescent substrate	Thermo Fisher Scientific	Cat#34580
Deposited data		
Affinity-based mass spectrometry	This study	Tables S1–S3, S5and S6
Experimental models: Organisms/strains		
Schizosaccharomyces pombe strains	This study	Table S8
Oligonucleotides		
Primers	This study	Table S9, also see (Cummings et al., 2015)
Recombinant DNA		
Plasmids		N/A
pFA6a-natMX6	(Hentges et al., 2005; Motamedi et al., 2004; Sato et al., 2005)	pFA6a-natMX6
pFA6a-hphMX6	(Hentges et al., 2005; Motamedi et al., 2004; Sato et al., 2005)	pFA6a-hphMX6
pFA6a-GFP(S65T)-kanMX6	(Bahler et al., 1998)	pFA6a-GFP(S65T)-kanMX6
pFA6a-TAP-hphMX6	(Motamedi et al., 2004)	pFA6a-TAP-hphMX6

(*Continued on next page*)

Continued

REAGENT or RESOURCE	SOURCE	IDENTIFIER
pFA6a-13Myc-natMX6	(Motamedi et al., 2004)	pFA6a-13Myc-natMX6
pFA6a-3FLAG-hphMX6	A gift from the Moazed Lab	pFA6a-3FLAG-hphMX6
Software and algorithms		
ImageJ (Fiji) with 2D parallel iterative deconvolution plugin	NIH	RRID:SCR_002285
Graphpad prism 7 software	Graphpad	RRID:SCR_002798
Microsoft excel	Microsoft	RRID:SCR_016137
Slide book software version 4.2	Intelligent Imaging Innovations Inc.	https://microscopy.jhmi.edu/Learn/refman/3i/SlideBook4.2UsersManual.pdf
In-house mass spectrometry data analysis	(Huttlin et al., 2010)	(Huttlin et al., 2010)
COMET	(Eng et al., 2013)	(Eng et al., 2013)
AnGeLi: Analysis of gene lists	http://bahlerweb.cs.ucl.ac.uk/cgi-bin/GLA/GLA_input	http://bahlerweb.cs.ucl.ac.uk/cgi-bin/GLA/GLA_input
Phyre2 web portal	(Kelley et al., 2015)	(Kelley et al., 2015)
Other		
MagNA lyzer instrument	Roche	Cat# 03,358,968,001
Olympus iX81 spinning disk deconvolution microscope	Olympus	https://www.olympus-lifescience.com/data/olympusmicro/brochures/pdfs/ix81.pdf?rev=EABE
QExactive Mass spectrometer	Thermo Fisher Scientific	Cat# IQLAAEGAAPFALGMBDK

RESOURCE AVAILABILITY

Lead contact

Further information and requests for resources and reagents should be directed to and will be fulfilled by the Lead Contact, Dr. Mo Motamedi, mmotamedi@hms.harvard.edu.

Materials availability

Requested materials are available from the Lead Contact.

Data and code availability

All relevant data are included in the present article and its supplemental information or are available from the Lead Contact upon request. The paper does not report original code. Any additional information required to reanalyze the data reported in this work paper is available from the Lead Contact upon request.

EXPERIMENTAL MODEL AND SUBJECT DETAILS

Strain construction

The origin and genotype of the strains used in this study are outlined in Table S8. *S. cerevisiae* and *S. pombe* strains were constructed using standard yeast transformation methods (Bahler et al., 1998). To construct the deletion strains, the entire coding region of the gene is replaced with a drug cassette. C-terminally tagged proteins were constructed by adding the tag (MYC, TAP, GFP) in-frame to the C terminus of the gene prior to its stop codon (Cummings et al., 2015). All strains carrying tagged proteins were tested in phenotypic assays to confirm the protein's *in vivo* activity compared to wild-type and deletion strains. Only functional, C-terminally tagged proteins whose expressions are under the control of their native promoters were used in this paper. List of all primers used for tagging or deleting genes in this paper can be found in (Cummings et al., 2015).

Yeast growth assays, amino acid starvation and amino acid supplementation

Fission yeast cells were grown at 32°C in Yeast Extract supplemented with Adenine (YEA) or synthetic minimal media (EMM) supplemented with 0.225 g/L adenine, histidine, leucine, lysine and uracil (EMM +aa) (Alfa, 1993). For growth assays, the starting OD_{600} of all strains was between 0.2 and 0.3. This culture was prepared by inoculating pre-warmed (32°C) EMM + aa media with log phase cells (OD_{600} of 1–2).

Cell growth was then measured by OD_{600} measurements post-inoculation. Amino acid starvation was achieved by first growing the cells in EMM + aa to log phase (OD_{600} roughly 1.0), then washing cell pellets twice in 32°C EMM lacking the aforementioned supplements (EMM - aa) and resuspending them in the same volume of pre-warmed (32°C) EMM - aa. Cells were kept at 32°C for indicated times post amino acid starvation. To assay growth and TORC1 activation after amino acid starvation, cells were first starved for amino acids for 140 min, then spun and resuspended in the same volume of pre-warmed EMM + aa media and incubated at 32°C for indicated time points. For Western blot analyses, 5 mL of each culture was harvested from which protein extracts were prepared using trichloroacetic acid (TCA) protein extraction (see below). Also, for determining the Rapamycin effect, EMM + aa cultures containing 0, 125, or 150 ng/mL of Rapamycin were used. After 90 min, 5 mL of Rapamycin treated cells was harvested from which protein extracts were prepared using trichloroacetic acid (TCA) protein extraction (see below).

METHOD DETAILS

Tandem affinity purification

The tandem affinity purification (TAP) tag used in this study is composed of two protein A repeats and a calmodulin binding peptide separated by recognition site for the tobacco etch virus (TEV) protease (Rigaut et al., 1999). Six liters of *S. pombe* cells was grown at 32°C in EMM + aa to an OD_{600} between 2 and 2.3, yielding about 14 g of pellet. Cell pellets were then resuspended in lysis buffer (10 mM Tris–HCl (pH 8), 150 mM NaCl, 20 mM $MgCl_2$, 0.1% NP40, 1 mM DTT, 10 mM PMSF, 1 complete Mini protease inhibitor tablet (Roche)/50mL lysis buffer and 1 phosphatase inhibitor tablet (Roche)/10mL of lysis buffer) at a ratio of 0.25 g of cell pellet in 0.4 mL of lysis buffer. Cell suspensions were frozen directly in liquid nitrogen and the frozen pellets were lysed using a Qiagen TissueLyser II (5 × 2 min at 20 Hertz). The lysis chamber was dipped in liquid nitrogen for 3–5 min in between each cycle. Two-step Bhd1-TAP and SPAC30C2.07 (Fnp1)-TAP purifications were performed as described previously (Motamedi et al., 2004). All TEV cleavage steps were done at 4°C overnight. Roughly 1/3 of the eluate was run on a 10% polyacrylamide gel and stained with silver; the remaining 2/3 was submitted for mass spectrometric analysis. All one-step TAP purifications were performed using roughly 7 g of log phase cells collected and lysed as described above. TAP-tagged proteins were immunoprecipitated with 5 uL IgG beads/g of cells for 4 h at 4°C. Beads were washed five times with 5 mL lysis buffer. Proteins were eluted by incubating beads in 500 mM NH_4OH for 20 min at 37°C. Eluted proteins were either dried for 1hr in vacuum and analyzed by Western blotting and silver staining using 8% SDS-PAGE gels, or were run on a gel, stained with colloidal Coomassie and subjected to in-gel digestion for mass spectrometric analysis.

Liquid chromatography and tandem mass spectrometry

Label-free mass spectrometry analysis was performed using either GeLC-MS/MS or in solution digestion, as specified in the main text. The GeLC-MS/MS analysis was performed as described previously (Paulo, 2016). In solution digestion was performed on-bead from immunoprecipitations by first adding 20 µL of 8 M urea, 100 mM EPPS pH 8.5 to the immunoprecipitates followed by 5mM TCEP and incubation for 15 min at room temperature. Next, 10 mM of iodoacetamide was added for 15min at room temperature in the dark, followed by 15 mM DTT to consume any unreacted iodoacetamide. We added 180µL of 100 mM EPPS pH 8.5 were added to reduce the urea concentration to <1 M, followed by adding 1 µg of trypsin, and incubating the mixture at 37°C for 6 h. Next, the solution was acidified to stop the digestion reaction with 2% formic acid. All peptides were desalted via StageTip, dried via vacuum centrifugation, and reconstituted in 5% acetonitrile, 5% formic acid prior to LC-MS/MS processing.

Our mass spectrometry data were collected using a Q Exactive mass spectrometer (Thermo Fisher Scientific, San Jose, CA) coupled with a Famos Autosampler (LC Packings) and an Accela600 liquid chromatography (LC) pump (Thermo Fisher Scientific). Peptides were separated on a 100 µm inner diameter microcapillary column packed with ~25 cm of Accucore C18 resin (2.6 µm, 150 Å, Thermo Fisher Scientific). For each analysis, we loaded ~1 µg of total eluted protein onto the column.

Peptides were separated using a 1 h gradient of 5–25% acetonitrile in 0.125% formic acid with a flow rate of ~300 nL/min. The scan sequence began with an Orbitrap MS1 spectrum with the following parameters: resolution 70,000, scan range 300–1500 Th, automatic gain control (AGC) target 1 × 105, maximum injection time 250 ms, and centroid spectrum data type. We selected the top twenty precursors for MS2 analysis which consisted of HCD high-energy collision dissociation with the following parameters: resolution 17,500, AGC 1 × 10^5, maximum injection time 60 ms, isolation window 2 Th, normalized collision energy

(NCE) 30, and centroid spectrum data type. The underfill ratio was set at 1%, which corresponds to a 1.1×10^4 intensity threshold. In addition, unassigned and singly charged species were excluded from MS^2 analysis and dynamic exclusion was set to automatic.

Proteomic data analysis

Mass spectra were processed using a Sequest-based in-house software pipeline and searched against the UniProt *S. pombe* database (Huttlin et al., 2010). Spectra were converted to mzXML using a modified version of ReAdW.exe. Database searching was performed using a 50-ppm precursor ion tolerance for total protein level analysis. The product ion tolerance was set to 0.03 Da. These wide mass tolerance windows were chosen to maximize sensitivity in conjunction with Sequest searches and linear discriminant analysis (Beausoleil et al., 2006; Huttlin et al., 2010). Oxidation of methionine residues (+15.995 Da) was set as a variable modification. Peptide-spectrum matches (PSMs) were adjusted to a 1% false discovery rate (FDR) (Elias and Gygi, 2007, 2010). PSM filtering was performed using a linear discriminant analysis, as described previously (Huttlin et al., 2010), while considering the following parameters: XCorr, ΔCn, missed cleavages, peptide length, charge state, and precursor mass accuracy. PSMs were identified, quantified, and collapsed to a 1% peptide false discovery rate (FDR) and then collapsed further to a final protein-level FDR of 1%. Moreover, protein assembly was guided by principles of parsimony to produce the smallest set of proteins necessary to account for all observed peptides.

Structure-based sequence alignments

A structure-based sequence alignment of the human FNIP2 sequence alignment to *S. pombe*Fnp1 was generated with the Phyre2 web portal (Kelley et al., 2015). To achieve correct alignment, we extracted the hFNIP2 structure from the FLCN-FNIP2-Rag-Ragulator complex (Shen et al., 2019) (pdb ID 6ULG.N) and performed the homology alignment in phyre2's one-to-one threading mode set to global alignment. The homology prediction returned 29% sequence identity with 99.80% confidence.

Protein co-immunoprecipitation assays

Four-hundred mL cultures of different *S. pombe* strains were grown in synthetic minimal media (EMM) supplemented with 0.225 g/L adenine, histidine, leucine, lysine and uracil (EMM + aa) at 32°C to an optical density (OD_{600}) of 1.0. 200 mL of this culture was starved for amino acids by washing twice and resuspending the cells in the same volume of pre-warmed (32°C) EMM without amino acids (EMM-aa) and incubating the cells at 32°C for 90 min before harvesting. Cell pellets were frozen in liquid nitrogen and lysed by glass beads in immunoprecipitation buffer (50 mM Tris–HCl pH 7.5, 200 mM NaCl, 5 mM EDTA, 0.5% NP40, 1 mM PMSF, 1 mM DTT and 1 mM benzamidine (0.25g of cells/0.04mL lysis buffer), 1 complete Mini protease inhibitor tablet (Roche)/50mL lysis buffer). Lysates were cleared by centrifugation, normalized for total protein by Bradford and immunoprecipitated with 10ul of IgG or FLAG beads for every 0.25 g of frozen cells, or 3ul of MYC antibody for 2 h at 4°C. Beads were washed three times with immunoprecipitation buffer plus protease inhibitors. Eluted proteins and input extracts were analyzed by standard immunoblotting procedures, using horseradish peroxidase-conjugated anti-peroxidase (PAP, Sigma, 1:2000), FLAG (Sigma, A8592, 1:2000) or MYC (Covance, 9E10, 1:2000), following standard procedures. For the co-immunoprecipitation experiments of TAP-tagged proteins, TAP was immunoprecipitated first followed by probing with MYC or anti-Vma2 antibody.

Fluorescence microscopy of GFP-tagged proteins

Cells were grown at 32°C in EMM + aa to log phase (OD_{600} = 1). To visualize protein localization after amino acid starvation, cells were washed twice and resuspended in pre-warmed EMM –aa media for 90 min. Green fluorescent protein (GFP) tag was used to visualize GFP-tagged Bhd1 and Fnp1 proteins (FITC filter, 100-1000msec). FM4-64 dye was used to stain the vacuole membrane (RFP filter, 10-100msec) as described previously (Valbuena et al., 2012a). Cell images were captured using an Olympus IX81 fluorescence microscope, equipped with Hamamatsu EM-CCD digital camera and processed using Slidebook software. FIJI program was used to measure the intensity of fluorescence. 2D Parallel Iterative Deconvolution plugin for Fiji program was used to perform the deconvolution of the fluorescence images.

Vacuolar pH determination

LysoSensor Green DND-189 dye (Thermo Fisher Scientific) was used to determine relative vacuolar pH (FITC filter) in different strains and growth conditions. 1 mL of exponentially growing *S. pombe* cells

(OD_{600} of 0.8–1.0) in EMM + aa were incubated with 1 mM DND-189 and 40 mM HEPES pH 7.9 for 5 min at 25°C and then washed three times in EMM + aa at room temperature. A culture of wild-type cells incubated with the V-ATPase inhibitor bafilomycin (10 nM for 4–5 min at 32°C) was used as a control for alkalinized vacuoles. Cell images were taken and processed as describe above (Imaging). To visualize live cells, differential interference contrast (DIC) was used, for vacuolar pH FITC (DND 189) was used, and for vacuoles, red filter (FM4-64) was used. Exposure times ranged between 200 and 800msec.

Trichloroacetic acid (TCA) protein extracts and immunoblot analysis

Protein extracts were obtained using trichloroacetic acid (TCA) extraction as described previously (Motamedi et al., 2008). Briefly, cell pellets, prepared from 5 mL of logarithmically growing cells (32°C in EMM + aa medium, $OD_{600} \sim 0.7–1$) frozen in liquid nitrogen, were resuspended in 0.5 mL of cold TCA buffer (20mM Tris (pH 8.0); 50 mM ammonium acetate; 2 mM EDTA; 2 mM PMSF; 2 mM Leupeptin; and 2 mM aprotinin), 0.5 mL of cold 30% TCA, and 0.5 mL of cold glass beads. Pellets were lysed in MagNA Lyser (Roche) instrument (3 × 30 s at 6000rpm with a 3 min on ice incubation in between). After lysis, the extracts were centrifuged at 20,000 rcf for 5 min and the resulting pellets were washed once in acetone. Acetone was removed and the protein pellets were resuspended in 40 µL TRIS buffer (0.1 M Tris-HCl pH 8.0.1 mM EDTA, 1%SDS) and 10 µL 5X loading buffer (containing 1 mM DTT and 1 mM PMSF) and boiled at 100°C for 5 min. Protein extracts were separated by SDS-PAGE (12%), transferred onto a nitrocellulose filter and analyzed by Western blot using anti-Phospho-S6 Ribosomal protein (Ser235/236) antibody (Cell Signaling, 4858). Tubulin was used as the protein loading control (Sigma, T6074). Immunoblots were developed using the enhanced chemiluminescence procedure.

S. cerevisiae growth C = conditions and protein co-immunoprecipitation assay

Fifty ml cultures of WT (BY4741) and Lst7-TAP *S. cerevisiae* strains were grown in minimal synthetic media (SD) with amino acids (synthetic complete medium, SC) at 32°C to an OD_{600} of 1.0. 25mL of this culture was starved for amino acids by washing twice and resuspending in the same volume of pre-warmed (30°C) media lacking amino acids (SD) for 90 min before harvesting. Cell pellets were flash-frozen in liquid nitrogen and lysed by glass beads in immunoprecipitation buffer (50mM Tris–HCl pH 7.5, 200mM NaCl, 5mM EDTA, 0.5% NP40, 1mM PMSF, 1mM DTT and 1mM benzamidine [0.25g cells/0.04mL lysis buffer]). Lysates were cleared by centrifugation, normalized for total protein by Bradford and were immunoprecipitated with 10µL of TAP beads for every 0.25 g of cells for 2 h at 4°C. Beads were washed three times with immunoprecipitation buffer plus protease inhibitors. Eluted proteins and input extracts were analyzed by standard immunoblotting procedures, using horseradish peroxidase-conjugated anti-peroxidase (PAP, Sigma, 1:2000) and rabbit polyclonal anti-Vma2 antibody (13D11B2, Abcam Ab113684, 1:2000).

Rapamycin, bafilomycin and alkaline pH plate sensitivity assays by serial dilution

To assay Rapamycin sensitivity, 10 mL of *S. pombe* cells were grown in EMM + aa or YEA at 32°C to an OD_{600} 0.8–1.2. 10-fold serial dilutions for each culture were then spotted on EMM + aa or YEA plates with or without 200ng/mL of Rapamycin. Similarly, dilutions were also prepared and spotted on EMM + aa or YEA plates with or without 700 nM of Bafilomycin and 200 mM $CaCl_2$. To analyze lack of growth on alkaline plates, *S. pombe* strains were grown and spotted on YEA media pH 9 by adding sodium phosphate monobasic (NaH_2PO_4). Plates were incubated at 32°C for 2–5 days. Images were captured with GEL DOC XR + system (white light illuminator).

QUANTIFICATION AND STATISTICAL ANALYSIS

Where applicable, statistical parameters including sample size, precision measures standard deviation (SD) and statistical significance are reported in the Figures and corresponding Figure Legends. Results are expressed as means of at least three independent experiments. Error bars represent the standard deviation of at least three independent biological replicates. Statistical significance was determined by Student's t-test (paired-data analysis). p values ≤ 0.05 (*) were considered to be statistically significant. For imaging, FIJI program was used to measure the intensity of fluorescence and the data from three independent experiments were exported to Excel for analysis. In Figure S5E, Fiji was used for densitometric analysis of immunoblots. Intensity values were exported to Excel, and P-Rps6 band intensities were normalized both to t = 0min and the tubulin loading control. An unpaired, two-tailed Student's t-test was used to

assess the significance of the difference between WT and *bhd1Δ*mean intensities at the 40min timepoint. A *p* value of less than 0.05 was deemed as significant. Pombase website https://www.pombase.org/was used as the comprehensive database for *S. pombe* analyses. To identify Gene Ontology (GO) biological processes (BPs) enriched in our datasets, we used AnGeLi, developed by the Bahler group specifically for the fission yeast. See http://bahlerweb.cs.ucl.ac.uk/cgi-bin/GLA/GLA_input. For all analyses, we used the default settings to identify BPs were enriched in our datasets.